IEEE Access
Multidisciplinary | Rapid Review | Open Access Journal

Received 7 February 2023, accepted 22 February 2023, date of publication 27 February 2023, date of current version 2 March 2023.

Digital Object Identifier 10.1109/ACCESS.2023.3249294

RESEARCH ARTICLE

An Enhanced Pignistic Transformation-Based Fusion Scheme With Applications in Image Segmentation

JIAXU ZHANG[1,2], XIAOJIAN MA[1], TINGTING SONG[3], (Member, IEEE), AO WANG[1], AND YUHUA LIN[1]

[1]College of Science, Northeast Forestry University, Harbin 150000, China
[2]School of Electronics and Communication Engineering, Sun Yat-sen University, Shenzhen 518000, China
[3]Department of Electrical and Electronic Engineering, The University of Melbourne, Parkville, VIC 3010, Australia

Corresponding author: Xiaojian Ma (mxjzy@nefu.edu.cn)

This work was supported in part by the Fundamental Research Funds for the Central Universities under Grant 2572018BC21, and in part by the College Students Innovations Special Project—Northeast Forestry University of China under Grant 202110225372.

ABSTRACT The traditional Pignistic transformation is limited in the context of ''betting'', which faces information loss and is inconvenient for multi-source information fusion. To tackle this challenge, an Enhanced Pignistic transformation is proposed for the first time. New divergence and information volume measures are tailor-made for the enhanced Pignistic probability, and a novel information fusion algorithm is developed. To further prove the fusion algorithm's advantages in conflict management, it is applied in a new semi-automatic image segmentation scheme. Two uncertain decision-support techniques named adaptive belief assignment and scalable information extraction are raised, and a fuzzy heuristic refinement algorithm is conducted, fulfilling the gap between evidential decision-making and segmentation refinement. Experimental analysis shows the proposed segmentation algorithm is superior on four metrics each and can enhance the robustness of foreground segmentation, indicating the effectiveness of the proposal in solving the decision inaccuracy of evidential segmentation schemes.

INDEX TERMS Enhanced Pignistic transformation, multi-source information fusion, belief hellinger distance, semi-automatic image segmentation, uncertain decision-support, heuristic refinement.

I. INTRODUCTION AND RELATED WORKS

Multi-source information fusion is a kind of technique that supports multi-sensors to make objective and accurate decisions, which is firstly applied in military fields [1]. In recent years, with the rapid development of information technology and knowledge-based artificial intelligence, the application of multi-source information fusion has been extended to civil decision-making [2], [3], [4]. Evidence theory is a widely accepted decision-making structure to solve multi-source information fusion problems [5], which has the capability to express uncertainty and ignorance when making decisions [6], [7], [8].

The associate editor coordinating the review of this manuscript and approving it for publication was Yu-Da Lin.

Even though evidence theory has the merits mentioned above, it still faces challenges. When the multi-source information contains conflicting data, counterintuitive decisions will be produced [9]. To tackle this problem, plenty of methods based on evidential distance have been proposed to model the conflict degree. For example, Jousselme et al. introduced a distance between two Basic Probability Assignments (BPAs), which gives the similarity between subsets [10]. However, Jousselme's distance does not consider the number of elements in one subset. As a result, even if the subset has changed, the distance between the two pieces of evidence does not change. To solve this problem, a similarity coefficient matrix was presented to model the cardinality of each subset, and a distance-based similarity coefficient matrix was designed. Recently, Xiao proposed an

evidential fusion framework utilizing Belief Jensen-Shannon divergence [11]. Zhu et. al. also devised evidential fusion algorithms using Belief Hellinger distance and Generalized Belief Renyi divergence [6], [12]. However, the effects of Xiao's and Zhu's methods on decision accuracy are still in need of improvement. In this study, a new evidential fusion algorithm is devised, which takes a new perspective to tackle the multi-source information conflict.

In addition to conflict management, probability reconstruction is yet another research hot spot in evidence theory [13]. The Transferable Belief Model is a double-layer structured probability regeneration framework [14], which has gained wide reputation in failure prediction [15], target tracking [16] and clustering [17]. From this model, a belief regeneration approach named Pignistic transformation is developed. However, this transformation is limited in the context of ''betting'', thus it faces a loss of information [18], [19], which is inconvenient for evidential fusion. In earlier studies, [13] suggested it is its average reassignment strategy, which is rather conservative, results in the bad belief reallocation. But this viewpoint cannot fully explain the loss of information. Even though plenty of improved frameworks for probability regeneration have been researched and well studied, such as [13], [20], [21], and [22], the mentioned limitation is still ignored [13], [23]. Recently, Zhu et. al. proposed the PSD Pignistic probability [19] to manage the mentioned information loss, but as pointed out in this paper, their PSD Pignistic probability faces another problem, i.e. the probability degeneration. Therefore, to tackle the information loss and avoid the probability degeneration, this article starts from the intrinsic properties of Pignistic transformation, and resolves its problem by redesigning its probability mapping. Through theoretical analysis, a new decision probability transformation named Enhanced Pignistic transformation is constructed. Then the mathematical framework on its 1) divergence and 2) information volume measure is developed, which are named as Enhanced Pignistic Hellinger Distance (EPHD) and Enhanced Pignistc Deng Entropy (EPDeng Entropy) respectively. Based on the two measures, a new conflict-based information fusion algorithm is firstly conducted.

Except for the theoretical justifications described above, the evidence theory has also been intensively studied in various real-world applications [24], [25]. However, only a little amount of literature relates to evidential semi-automatic image segmentation [26]. Current evidence theory-based methods face two challenges. The first one is the information conflict. For example, in [27], an iterative segmentation framework combining Gaussian Mixture Model and spatial information is devised. However, the conflict between BPAs is ignored, which limits its decision accuracy. The second problem is the severe false segmentation. For instance, Chaabane et al. constructed a segmentation algorithm using evidence theory [28]. However, this approach lacks robustness due to its simple pixel-level feature extraction. As far as we know, the two challenges in evidential semi-automatic segmentation have not been researched and resolved by now. Consequently, this paper addresses the two challenges by proposing a new semi-automatic image segmentation algorithm applying evidential decision-making. To tackle the first challenge, the newly devised information fusion algorithm is embedded into the fusion process. To manage the second challenge, a heuristic refinement algorithm is proposed, which embraces the evidence theory and fuzzy decision-making. Also, two decision-making techniques with uncertain information named adaptive belief generation and scalable information extraction are designed for BPA generation.

In summary, the contributions in this study are three-folds:

- This paper devises an Enhanced Pignistic transformation-based evidential fusion algorithm. The Enhanced Pignistic transformation can help to alleviate the loss of information without probability degeneration. The Enhanced Pignistic Hellinger Distance (EPHD) and Enhanced Pignistc Deng Entropy (EPDeng Entropy) are also deduced. Then the new information fusion framework is applied in the proposed semi-automatic segmentation algorithm.
- A coarse-to-fine evidential image segmentation framework is constructed. It resolves the information conflict through the proposed evidential fusion scheme, and also improves the segmentation quality via two uncertain decision-support techniques, i.e., adaptive belief assignment and scalable information extraction.
- A fuzzy heuristic refinement algorithm is proposed. It fills the gap between segmentation refinement and evidential fuzzy decision-making.

This paper is organized as below. Section II sheds light on the preliminaries of evidence theory. Section III describes the proposed multi-source information fusion algorithm based on Enhanced Pignistic transformation at full length. Section IV introduces the new semi-automatic image segmentation algorithm, which embeds the proposed information fusion structure. In Section V, this segmentation approach is tested on two standard datasets, and is compared with state-of-the-art algorithms. An analysis of the innovations' advantages is also given in this section. Finally, concise conclusions are drawn in Section VI.

II. BACKGROUND KNOWLEDGE OF D-S EVIDENCE THEORY

In this section, some preliminaries with respect to D-S evidence theory are concisely introduced.

Like the Bayesian theory, it is essential to develop the frame of discernment (FOD) for evidence theory [29]. This mathematical structure is used to specify all the issues to be discriminated. Assume that Θ is a set that includes exclusive events, i.e. $\Theta = \{\eta_1, \eta_2, \ldots, \eta_M\}$, $\eta_i \neq \eta_j$, $\forall i \neq j$, $i, j = \{1, 2, \ldots, M\}$, then Θ is defined as FOD, whose power set is denoted as 2^Θ. It can be clearly seen that $2^\Theta = \{\emptyset, \eta_1, \eta_2, \ldots, \eta_M, \eta_1 \cup \eta_2, \ldots, \eta_{M-1} \cup \eta_M, \ldots, \Theta\}$. Each element in Θ is referred to as a focal element, while each element in 2^Θ is named as a hypothesis. The hypothesis with cardinality being 1 is called as a singleton.

Another background work is to construct the basic probability assignment (BPA), which configures the representation of "certain" and "uncertain" in evidence theory [23]. Assume that Θ is FOD, m is a mapping which satisfies: $2^{\Theta} \rightarrow [0, 1]$, then m with following properties is defined as BPA:

$$\begin{cases} m(\emptyset) = 0 \\ \sum_{\eta} m(\eta) = 1, \eta \in 2^{\Theta} \end{cases} \tag{1}$$

Dempster's combination rule [30] is then required to break BPAs down into uncertain degrees, which facilitates the following decision-making process. Suppose $\Theta = \{\eta_1, \eta_2, \ldots, \eta_M\}$, $m_1, \ldots, m_N$ are N sets of BPAs, then the Dempster combination rule can be expressed as Eqs. (2):

$$\begin{cases} m(\emptyset) = 0 \\ m(\eta_j) = \frac{1}{1-K} \sum_{\cap\eta=\eta_j} \prod_{1\leqslant s\leqslant N} m_s(\eta_j), \eta_j \in 2^{\Theta} \end{cases} \tag{2}$$

where $K = \sum_{\cap\eta=\emptyset} \prod_{1\leqslant s\leqslant N} m_s(\eta_j)$ is called conflict coefficient.

In addition, via Pignistic transformation, BPAs can be converted into Pignistic probabilities for "betting". According to [31], suppose that m is the BPA, Θ is FOD, the Pignistic transformation for singletons is formed with Eq. (3):

$$BetP(\eta) = \sum_{\psi \in 2^{\Theta}} m(\psi) \frac{|\eta \cap \psi|}{|\psi|} \tag{3}$$

where $|*|$ is the cardinality of $*$, $\eta \in \Theta$ (note that if in line with the definition of Xiao [37], this transformation is defined as Pignistic transformation for singletons).

Recently, Zhu et. al. [19] proposed the PSD Pignistic transformation as a bijection from 2^{Θ} to 2^{Θ} to eliminate the information loss of the traditional Pignistic transformation:

$$PBetP(\eta) = \sum_{\psi \in 2^{\Theta}} m(\psi) \frac{2^{|\eta\cap\psi|} - 1}{2^{|\psi|} - 1} \tag{4}$$

where $\eta \in 2^{\Theta}$. But as analyzed in this paper, this transformation confronts probability degeneration, which has been investigated and improved in the following section.

As a metric measuring the evidential distance, Belief Hellinger Distance has been devised for multi-source information fusion [6]. Suppose that m_1 and m_2 are two sets of BPAs respectively, Θ is the FOD, then the Belief Hellinger Distance between m_1 and m_2 can be calculated as below:

$$BH_{1,2} = \frac{1}{\sqrt{2}} \sqrt{\sum_{\eta \in 2^{\Theta}} \frac{\left(\sqrt{m_1(\eta)} - \sqrt{m_2(\eta)}\right)^2}{2^{|\eta|} - 1}} \tag{5}$$

where $|\eta|$ is the cardinality of η.

Last but not least, the Deng entropy is established for measuring the degree of information volume in pieces of evidence [32]. Denote m is a BPA function, the Deng entropy can therefore be characterized as this equation:

$$DE = -\sum_{\eta \in 2^{\Theta}} m(\eta) \log \frac{m(\eta)}{2^{|\eta|} - 1} \tag{6}$$

where $|\eta|$ manifests the cardinality of η.

III. THE ENHANCED PIGNISTIC TRANSFORMATION AND PROPOSED EVIDENTIAL FUSION ALGORITHM

In this section, the proposed conflict-based evidential fusion algorithm is described at full length. The Enhanced *BetP* functions, Enhanced Pignistic Hellinger Distance (EPHD) and Enhanced Pignistic Deng Entropy (EPDeng Entropy) are devised separately. Finally, a conflict fusion example is involved for the performance verification.

A. THE ENHANCED PIGNISTIC TRANSFORMATION FOR MULTI-SOURCE INFORMATION FUSION

In evidence theory, the Pignsistic transformation [31] is widely used for "betting" [33]. However, the "betting frame" includes singletons only, which may result in information loss. The refined probability, PSD Pignistic probability [19], mitigates the information loss but faces probability degeneration, and its corresponding information fusion algorithm lacks efficiency. Therefore, before the new evidential fusion scheme is proposed, the definition of Enhanced Pignistic transformation is provided first.

Following the description by Smets [31], [35], before doing the Pignistic transformation for a "betting", i.e. a forced decision on limited hypotheses, one should build the "betting frame" first, whose semantic is " a list of alternatives on which the bet must be made". In the light of [34], the "betting frame" contains all of the "atoms" waiting for a choice. For example, in [36], the FOD $\Theta = \{positive, negative\}$, and the BPA is construced on $2^{\Theta} = \{\emptyset, positive, negative, \Theta\}$, then the "betting frame" is $\{positive, negative\}$. Next, the BPA is broken down to the atoms in the "betting frame" through Pignistic transformation [34]. In other words, the Pignistic probabilities generated via Eq. (3) are *Bayesian*, i.e. the probabilities are reassigned only on singletons [41], [42].

However, although the formed *Bayesian* probability is suitable for a "betting", it faces a loss of belief representation on multi-singletons comparing with the original BPA, which has been criticized by [18] and [19]. To eliminate the mentioned information loss, in [19] the PSD Pignistic probability is proposed, which is a bijection from 2^{Θ} to 2^{Θ}. In other words, the PSD Pignistic transformation directly added all the multi-singletons into Smets' "betting frame". But this transformation faces probability degeneration, which breaks Smets' wish to construct a real probability and might be inconvenient for multi-source information fusion. An example is used to illustrate this shortcoming.

Example 1: Suppose m is a piece of BPA with $\Theta = \{\{a\}, \{b\}, \{c\}\}$:

$$\begin{aligned} m(\{a\}) &= 0.57, \quad m(\{b\}) = 0.07 \\ m(\{c\}) &= 0.00, \quad m(\{a, c\}) = 0.36 \end{aligned} \tag{7}$$

Counterintuative results will emerge if Zhu's PSD Pignistic transformation is adopted for probability regeneration. To simplify description, this paper defines the **target hypothesis set** ζ as the generalization of Smets' "betting frame". Namely, we define $\Theta \subseteq \zeta \subseteq 2^\Theta$. In this instance, $\zeta = \{\{a\}, \{b\}, \{c\}, \{a, c\}\}$. Note that the hypothesis $\{a, c\}$ is a multi-singleton subset.

Then after adding multi-singletons to the generalized "betting frame", use the PSD Pignistic probability functions to distinguish the targets. With the aid of Eq. (4), the so-called PSD Pignistic probabilities, i.e. the *PBetP* functions, can be easily calculated as:

$$\begin{cases} PBetP(\{a\}) = m(\{a\}) + \dfrac{m(\{a, c\})}{3} = 0.690 \\ PBetP(\{b\}) = m(\{b\}) = 0.070 \\ PBetP(\{c\}) = m(\{c\}) + \dfrac{m(\{a, c\})}{3} = 0.120 \\ PBetP(\{a, c\}) = m(\{a\}) + m(\{c\}) + m(\{a, c\}) = 0.930 \end{cases} \tag{8}$$

It is clear that we have $\sum_\eta PBetP(\eta) = PBetP(\{a\}) + PBetP(\{b\}) + PBetP(\{c\}) + PBetP(\{a, c\}) = 1.810 > 1$, which violates the law of being a probability distribution. It means that the PSD Pignistic transformation in Eq.(4) fails to generate a genuine probability. In this paper, we claim such a transformed probability distribution has **degenerated**. But the Pignistic probability should be a classical probability measure and the summation of it should be 1 [5], thus the PSD Pignistic transformation breaks Smets' wish. Also, from a view of strict mathematics, it seems not rigorous to utilize a "degenerated" distribution to calculate entropy, divergence or other probability-based metrics, which might be inconvenient for multi-source information fusion.

Remark: Note that one may argue that why the concept of target hypothesis set is needed in multi-source information fusion, i.e. the generalized "betting frame" ζ. Two reasons are provided as behind.

- Firstly, consider that in the scenario of information fusion, it might be unavoidable that the information sources may choose a multi-singleton hypothesis as a final decision, especially when knowledge is extremely destitute, but Smets' "betting frame" is only devised for "betting", i.e. a forced decision on singletons [31], thus it does not take the multi-singletons into consideration, which may result in decision deviation.
- Secondly, although in [19], a formal definition on the generalzied betting frame is in lack, we think the PSD Pisgnistic probability can still be seen as an attempt on generalizing multi-singletons to Smets' "betting frame" for information loss management. But its betting frame is fixed as 2^Θ, which seems inflexible. This paper believes that in general, it is unnecessary to reassign beliefs to all the hypotheses in 2^Θ. That is also why we have $\Theta \subseteq \zeta \subseteq 2^\Theta$ rather than directly setting $\zeta = 2^\Theta$. If via BPAs, one can beforehand know that some multi-singletons are impossible events, then they can be excluded from the generalized "betting frame".

After the lead-in of target hypothesis set, we still remember in the context of "betting", the Pignistic probabilities converted from Pignistic transformation (3) are *Bayesian*. The excluding strategy on multi-singletons may cause information loss. The PSD Pignistic transformation [19] seems to be a more reasonable approach than the traditional Pignistic transformation, because it is a bijection from 2^Θ to 2^Θ, but it suffers from probability degeneration. To solve these problems, we think the new transformation should satisfy the two following properties:

1) To overcome the loss of information, the target hypothesis set ζ, whose elements are ready for belief reassignment, should generalize Smets' "betting frame" to multi-singletons. In other words, the relation $\Theta \subseteq \zeta \subseteq 2^\Theta$ should hold.
2) The new transformation should reassign beliefs to multi-singletons with probability degeneration avoided.

Therefore, the Enhanced Pignistic transformation is devised, which is illustrated as follows. Firstly, the $EBetP^*$ functions are calculated via Eq. (9):

$$EBetP^*(\eta) = \sum_{\psi \in \zeta, \eta \subseteq \psi} m(\psi) \frac{|\eta \cap \psi|}{|\psi|} \tag{9}$$

where $\eta \in \zeta$. The superscript "*" means the step of normalization is still in need. Then the Enhanced *BetP* (*EBetP*) functions are generated through Eq. (10):

$$EBetP(\eta) = \frac{EBetP^*(\eta)^2}{\sum_{\psi \in \zeta} EBetP^*(\psi)^2} \tag{10}$$

where $\eta \in \zeta$. Note that the *EBetP* functions only consider the belief from the supersets of each focal element. As for $\eta \in 2^\Theta - \zeta$, the *EBetP* functions are formed as behind:

$$EBetP(\eta) = 0 \tag{11}$$

Then using Eq. (9), (10) and (11), the definition of the Enhanced Pignistic transformation is described below.

Definition 1 (Enhanced Pignistic Transformation): Suppose the BPA is m, then the Enhanced Pignistic transformation means converting m functions into EBetP functions by utilizing Eq. (9), (10) and (11), which consequently forms Enhanced Pignistic probability.

Then the following theory is given, which is self-explantory and is fundamental to the Enhanced Pignistic probability.

Theorem 1: Thet EBetP functions obey the following properties:

(1) Nonnegativity: $EBetP(\eta) \geqslant 0, \forall \eta \in 2^\Theta$.

(2) Boundedness of summation: $\sum_{\eta} EBetP(\eta) = 1, \eta \in 2^{\Theta}$.

(3) Generalization: The Pignistic transformation (3) is a special case of the Enhanced Pignistic transformation. If one sets $\zeta = \Theta$*, the transformed EBetP* functions will be equivalent to BetP functions for all* $\eta \in \Theta$.

Note that the PSD Pignistic probability does not share the Generalization property in **Theorem 1**. Since in previous literature, plenty of studies have investigated the feasibility of using the Pignistic probabilities to develop uncertainty measure and divergence measure [19], thus we think that under the scenario of information fusion, the thought to employ the proposed *EBetP* functions to design its corresponding information volume and divergence measures serving as their own quantitative metrics on uncertainty and difference is rational. The Boundedness of summation property proven in **Theorem 1** can help us to reach this goal.

Then go a step further, if we supplementarily define $EBetP(\emptyset) = 0$, we can proof the Enhanced Pignistic functions share the same mathematical properties with BPAs:

$$\begin{cases} EBetP(\emptyset) = 0 \\ \sum_{\eta} EBetP(\eta) = 1, \eta \in 2^{\Theta} \end{cases} \tag{12}$$

Therefore, the *EBetP* functions can be *numerically* (or *mathematically*) fused through recently developed fusion rules without breaking the rules' mathematical properties. In the area of information fusion, many previous methods [6], [11] have tested the idea that employing modified BPA to pursue a more accurate decision-making results, and they have gained superior achievements. Therefore, to fuse the *EBetP* functions, which can be seen as modified BPAs, seems reasonable. Consequently, an inspiring thought is to use the constructed *EBetP* functions to manage information fusion problems. So we consider that the final goal of Section III should be organized as follows:

1) Utilize the devised *EBetP* function to develop its corresponding information volume and distance measures.
2) Consider the devised *EBetP* functions as modified BPAs, then construct a well-integrated multi-source information fusion algorithm based on its tailor-made divergence and information volume measures, which are employed to form the evidential weights.

Note that when doing the same fusion on the traditional Pignistic transformation (3) or its recent refined versions, such as [20], [21], and [22], considering their generated probabilities are *Bayesian*, which may exert an adverse effect on expressing information of ignorance, fusing their decision functions may result in deviated decisions. The PSD Pignistic probability can eliminate the information loss, notwithstanding, it faces probability degeneration. Comparing with the mentioned approaches, our method is more superior, because 1) the generalized "betting frame" contains the multi-singletons as the final decisions, hence the information loss is alleviated, and 2) the probability degeneration is avoided. As a result, we construct a new transformation that is from evidence to a new form of decision probability under the framework of Pignistic probability.

TABLE 1. The BPAs in Example 2.

Hypothesis	IS1: m_1	IS2: m_2	IS3: m_3	IS4: m_4	IS5: m_5
$\{F_1\}$	0.41	0.00	0.58	0.55	0.60
$\{F_2\}$	0.29	0.90	0.07	0.10	0.10
$\{F_3\}$	0.30	0.10	0.00	0.00	0.00
$\{F_1, F_3\}$	0.00	0.00	0.35	0.35	0.30

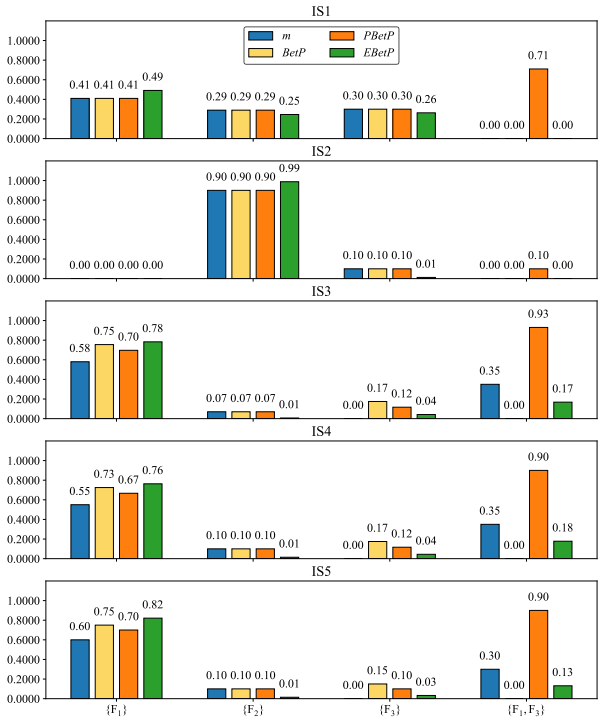

FIGURE 1. The BPAs, *BetP* functions, *PBetP* functions and *EBetP* functions from the standard checking example.

We still remember that the Enhanced Pignistic transformation is more superior since it solved the probability degeneration with efficiency. Next, we will illustrate that the proposed transformation is also more superior in keeping the decision consistency. Namely, the decision inconsistency means the decision semantics from the original BPAs are destroyed after beliefs transfer. This issue is illustrated by introducing the standard evidential fusion example devised in [6] and [11].

Example 2: This example sets five information sources (ISs) to identify the target fault among three kinds of faults. Note that IS2 makes a different decision from the rest, which is considered to be a piece of conflicting evidence. The five corresponding BPAs are listed in Table 1, with the target hypothesis set $\zeta = \{\{F_1\}, \{F_2\}, \{F_3\}, \{F_1, F_3\}\}$.

Then the BPAs, traditional *BetP* functions, *PBetP* functions and *EBetP* functions from the standard example in Table 1 are drawn in Fig. 1 respectively. (Similarly, note that the methods aiming to improve the Pignistic transformation

in [13], [20], [21], and [22], are devised for transforming *Bayesian* probabilities, thus they are beyond the scope of this paper. As a result, these methods are not involved.) In this figure, blue, yellow, orange and green bars are on behalf of the BPAs, *BetP* functions, *PBetP* functions and *EBetP* functions on each hypothesis. Except for the discussed probability degeneration, another interesting phenomenon can be observed, i.e. after the PSD Pignistic transformation, the intentional hypotheses changes to multi-singleton hypothesis $\{a, c\}$ except IS2 (i.e. $\arg\max_\eta m(\eta) \neq \arg\max_\eta PBetP(\eta)$). It indicates the original decision from BPAs has been distorted. That is counterintuitive, since if we consider the hypothesis with the maximum probability as the favored choice, then the original favored choice provided by the BPA has been thoroughly changed through this transformation. As for the traditional Pignistic transformation, it faces information loss since it reassigned zero-belief on multi-singletons. On the contrary, as a new decision probability, the *EBetP* functions have successfully maintained decision consistency. The proposed *EBetP* only considers the belief from the supersets of each target hypothesis, thus the "ignorance" will not expand too large when designating probability to multi-singleton subsets in *EBetP* functions.

Note that another unexpected but advantageous finding in Fig. 1 is that after the Enhanced Pignistic transformation, the new probability distribution becomes more uneven than the original BPAs and PSD Pignistic probabilities, i.e. $\max EBetP - \min EBetP$ is greater than (or equal to) $\max m - \min m$ and $\max PBetP - \min PBetP$, which can be explained by the simple but useful square operator in Eq. (10) beacuse it can be proven that $\frac{\max(m+\epsilon_{\max})^2 - \min(m+\epsilon_{\min})^2}{\sum_\eta (m(\eta)+\epsilon_\eta)^2} \geqslant \frac{\max m - \min m}{\sum_\eta m(\eta)}$ if ϵ_η is small enough, $\forall \eta \in \zeta$. It suggests that the devised *EBetP* distribution has a larger interclass difference, so each information source can be more confident in their intentional target. From the perspective of information fusion, it indicates the newly proposed *EBetP* functions not only have superiority in retaining decision consistency, but also are more distinguishable, then the final decisions in multi-source information fusion can be made easier.

B. THE ENHANCED PIGNISTIC HELLINGER DISTANCE, ENHANCED PIGNISTIC DENG ENTROPY

When fusing multi-source information, the generation of evidential weight is a key point to decision accuracy. However, earlier research mainly studied generating evidential weight by measuring the difference and information volume from BPAs or *BetP* functions [6], [11]. Since the proposed Enhanced Pignistic probability, current methods still lack evidential divergence measure and information volume measure specially designed for *EBetP* functions. To tackle this problem, Enhanced Pignistic Hellinger Distance (EPHD) and Enhanced Pignistic Deng Entropy (EPDeng Entropy) are originally devised in this article. A new conflict-based evidential fusion approach is conducted as well, whose performance is verified and compared with the standard checking example [6] mentioned in Section III-A.

Considering that the Belief Hellinger Distance has achieved high performance in multi-source information fusion and fault diagnosis [6], [8], to start with, the definition of Enhanced Pignistic Hellinger Distance, which is the first tailor-made quantitative divergence measure on *EBetP* functions, is given as below.

Definition 2 (Enhanced Pignistic Hellinger Distance): Suppose $EBetP_1$ and $EBetP_2$ are two sets of Enhanced Pignistic probability functions, Θ is the FOD, then the Enhanced Pignistic Hellinger Distance is defined as below:

$$EPHD_{1,2} = \frac{1}{\sqrt{2}} \sqrt{\sum_{\eta \in 2^\Theta} \frac{\left(\sqrt{EBetP_1(\eta)} - \sqrt{EBetP_2(\eta)}\right)^2}{2^{|\eta|} - 1}} \tag{13}$$

where $EPHD_{1,2}$ is short for $EPHD\,(EBetP_1, EBetP_2)$, $|\eta|$ is the number of events in η.

Note that if the focal elements share the same cardinality, i.e. $|\eta_i| = |\eta_j| = c, \forall \eta_i, \eta_j \in 2^\Theta$, the EPHD is also equivalent to this form:

$$EPHD_{1,2} = \frac{1}{\sqrt{2}} \frac{\|EBetP_1 - EBetP_2\|_{L_2}}{2^c - 1}. \tag{14}$$

where $\| * \|_{L_2}$ indicates the L_2 norm of $*$. Given the definition of *EPHD*, it is easy to derive the next theorem.

Theorem 2: The $EPHD_{1,2}$ satisfies the four following properties:

(1) Symmetry: $EPHD_{1,2} = EPHD_{2,1}$.

(2) Boundedness: $EPHD \in [0, 1]$.

(3) Nondegeneracy: $EPHD_{1,2} = 0$ if and only if $EBetP_1 = EBetP_2$.

(4) Limited Triangle Inequality: $EPHD_{1,2} + EPHD_{1,3} \geqslant EPHD_{2,3}$ if and only if $|\eta_i| = |\eta_j| = c, \forall \eta_i, \eta_j \in 2^\Theta$.

Proof: (1). It is clear that $\forall \eta \in 2^\Theta$, $(\sqrt{EBetP_1(\eta)} - \sqrt{EBetP_2(\eta)})^2 = (\sqrt{EBetP_2(\eta)} - \sqrt{EBetP_1(\eta)})^2$, thus we have

$$\begin{aligned} EPHD_{1,2} &= \frac{1}{\sqrt{2}} \sqrt{\sum_{\eta \in 2^\Theta} \frac{\left(\sqrt{EBetP_1(\eta)} - \sqrt{EBetP_2(\eta)}\right)^2}{2^{|\eta|} - 1}} \\ &= \frac{1}{\sqrt{2}} \sqrt{\sum_{\eta \in 2^\Theta} \frac{\left(\sqrt{EBetP_2(\eta)} - \sqrt{EBetP_1(\eta)}\right)^2}{2^{|\eta|} - 1}} \\ &= EPHD_{2,1}. \end{aligned}$$

Proof: (2). It is self-evident that $EPHD_{1,2} \geqslant 0$. Using the property that $EBetP \geqslant 0$ and note that $\forall \eta \in 2^\Theta$,

$$\begin{aligned} &\frac{\left(\sqrt{EBetP_1(\eta)} - \sqrt{EBetP_2(\eta)}\right)^2}{2^{|\eta|} - 1} \\ &\leqslant \frac{\left(\sqrt{EBetP_1(\eta)} - \sqrt{EBetP_2(\eta)}\right)^2}{1} \\ &\leqslant |EBetP_1(\eta)| + |EBetP_2(\eta)| \\ &= EBetP_1(\eta) + EBetP_2(\eta), \end{aligned}$$

Note that it has been proven that $\sum_{\eta} EBetP(\eta) = 1$, therefore

$$\begin{aligned} EPHD_{1,2} &\leqslant \frac{1}{\sqrt{2}}\sqrt{\sum_{\eta\in 2^{\Theta}} EBetP_1(\eta) + \sum_{\eta\in 2^{\Theta}} EBetP_2(\eta)} \\ &= \frac{1}{\sqrt{2}}\sqrt{1+1} \\ &= 1. \end{aligned}$$

Proof: (3). It is clear that when $EBetP_1 = EBetP_2$, there is $\sqrt{EBetP_1(\eta)} - \sqrt{EBetP_2(\eta)} = 0$, $\forall \eta \in 2^{\Theta}$, thus it is obvious that

$$\begin{aligned} EPHD_{1,2} &= \frac{1}{\sqrt{2}}\sqrt{\sum_{\eta\in 2^{\Theta}} \frac{\left(\sqrt{EBetP_1(\eta)} - \sqrt{EBetP_2(\eta)}\right)^2}{2^{|\eta|}-1}} \\ &= 0. \end{aligned}$$

Proof: (4). By using Cauchy-Schwartz inequality [43], we have

$$\begin{aligned} &\sqrt{2}\times EPHD_{1,2} + \sqrt{2}\times EPHD_{1,3} \\ &= \frac{\|EBetP_1 - EBetP_2\|_{L_2} + \|EBetP_1 - EBetP_3\|_{L_2}}{2^c - 1} \\ &\geqslant \frac{\|EBetP_2 - EBetP_3\|_{L_2}}{2^c - 1} \\ &= \sqrt{2}\times EPHD_{2,3}, \end{aligned}$$

therefore $EPHD_{1,2} + EPHD_{1,3} \geqslant EPHD_{2,3}$ if and only if $|\eta_i| = |\eta_j| = c$, $\forall \eta_i, \eta_j \in 2^{\Theta}$. □

In previous studies, the Deng entropy has shown both practicality and feasibility in fusing multi-source information [12]. Therefore, next, the definition of the Enhanced Pignistic Deng Entropy (EPDeng Entropy) is offered, which is the first belief entropy for an objective uncertainty measure on *EBetP* functions. The aim to propose EPDeng Entropy is to fill the gap between the Enhanced Pignistic probability and uncertainty estimation.

Definition 3 (Enhanced Pignistic Deng Entropy): Given the FOD Θ and the Enhanced Pignistic probability EBetP, the Enhanced Pignistic Deng Entropy is defined as:

$$EPDE = -\sum_{\eta\in 2^{\Theta}} EBetP(\eta)\log\frac{EBetP(\eta)}{2^{|\eta|}-1} \tag{15}$$

where $|\eta|$ implies the cardinal number of η.

In accordance with Moral-García and Abellán [45], the EPDeng Entropy can be decomposed as such a form:

$$\begin{aligned} EPDE = &-\sum_{\eta\in 2^{\Theta}} EBetP(\eta)\log EBetP(\eta) \\ &+ \sum_{\eta\in 2^{\Theta}} EBetP(\eta)\log(2^{|\eta|}-1) \end{aligned} \tag{16}$$

where the first term is called as the discord (conflict or randomness) part, and the second term is referred to as the non-specificity part. Note that the biggest difference between Deng entropy and the proposed entropy is at the conflict part. The proposed EPDeng Entropy attempts to estimate the information volume of *EBetP* functions.

After giving the definition of EPDeng Entropy, its properties are also provided.

Theorem 3: The proposed EPDeng Entropy satisfies:

(1) Nonnegativity: $EPDE \geqslant 0$.

(2) Probability Consistency: EPDeng Entropy will degenerate to Shannon Entropy [44] if 2^{Θ} contains singleton only, i.e. if $|\eta| = 1$, $\forall \eta \in 2^{\Theta}$, the equation below holds:

$$EPDE = -\sum_{\eta\in 2^{\Theta}} EBetP(\eta)\log EBetP(\eta).$$

(3) Set Consistency: EPDeng Entropy does not obey set consistency, that is because $EPDE = \log(2^{|\eta|}-1)$ is met rather than $\log(|\eta|)$ if there $\exists \eta \in 2^{\Theta}$, $|\eta| > 1$, $\forall \phi \in 2^{\Theta} - \{\eta\}$, s.t. $EBetP(\eta) = 1$, $EBetP(\phi) = 0$.

(4) Nonsubadditivity: EPDeng Entropy breaks the subadditivity. Suppose $EBetP^{X\times Y}$ is a joint EBetP function, and let $EBetP^{\downarrow X}$ and $EBetP^{\downarrow Y}$ be two sets of marginal EBetP functions respectively. If EPDeng Entropy satisfy subadditivity, then $EPDE_{EBetP^{X\times Y}} \leqslant EPDE_{EBetP^{\downarrow X}} + EPDE_{EBetP^{\downarrow Y}}$, $x \subset X$, $y \subset Y$.

(5) Nonadditivity: EPDeng Entropy also breaks the additivity. Suppose $EBetP^{X\times Y}$ is a joint EBetP function, and $EBetP^{\downarrow X}$ and $EBetP^{\downarrow Y}$ are two corresponding sets of marginal EBetP functions. If EPDeng Entropy satisfy additivity, then $EPDE_{EBetP^{X\times Y}} = EPDE_{EBetP^{\downarrow X}} + EPDE_{EBetP^{\downarrow Y}}$, $\eta \subset X$, $\psi \subset Y$.

Then the proof of this theorem is given.

Proof: (1). Note that $\forall \eta \in 2^{\Theta}$, $0 \leqslant EBetP(\eta) \leqslant 1$, $0 \leqslant \frac{EBetP(\eta)}{2^{|\eta|}-1} \leqslant 1$, $-\log\frac{EBetP(\eta)}{2^{|\eta|}-1} \geqslant 0$, therefore

$$EPDE = -\sum_{\eta\in 2^{\Theta}} EBetP(\eta)\log\frac{EBetP(\eta)}{2^{|\eta|}-1} \geqslant 0.$$

Proof: (2). If we set $\forall \eta \in 2^{\Theta}$, $|\eta| = 1$, thus we have $2^{|\eta|} - 1 = 1$, therefore the theorem holds.

Proof: (3). If there $\exists \eta \in 2^{\Theta}$, $\eta > 1$, $\forall \phi \in 2^{\Theta} - \{\eta\}$, s.t. $EBetP(\eta) = 1$, $EBetP(\phi) = 0$, and we also define $0 \times \log 0 = 0$, then EPDeng Entropy can be expanded as below:

$$\begin{aligned} EPDE = &-\sum_{\phi\in 2^{\Theta}-\{\eta\}} EBetP(\phi)\log\frac{EBetP(\phi)}{2^{|\phi|}-1} \\ &- EBetP(\eta)\log\frac{EBetP(\eta)}{2^{|\eta|}-1} \\ = &-\sum_{\phi\in 2^{\Theta}-\{\eta\}} 0\times\log\frac{0}{2^{\phi}-1} - 1\times\log\frac{1}{2^{|\eta|}-1} \\ = &\log(2^{|\eta|}-1) > \log(|\eta|). \end{aligned}$$

Therefore, EPDeng Entropy breaks the set consistency.

Proof: (4) An example is used to clarify this property.

Example 3: Denote the joint probability space $X \times Y$, marginal probability space $X = \{x_1, x_2\}$ and $Y =$

$\{y_1, y_2, y_3\}$. *Then the joint EBetP function is defined as*

$$EBetP^{X\times Y}(\{\eta_{11}, \eta_{12}, \eta_{21}\}) = 0.6,$$
$$EBetP^{X\times Y}(\{\eta_{13}, \eta_{23}\}) = 0.2,$$
$$EBetP^{X\times Y}(X \times Y) = 0.2.$$

where $\eta_{ij} = x_i y_j$. *Marginal EBetP functions are defined and calculated respectively*:

$$EBetP^{\downarrow X}(X) = 1.$$
$$EBetP^{\downarrow Y}(\{y_1, y_2\}) = 0.6, EBetP^{\downarrow Y}(\{y_3\}) = 0.2,$$
$$EBetP^{\downarrow Y}(Y) = 0.2.$$

Then the EPDeng Entropy of the three sets of EBetP functions are calculated as below:

$$EPDE_{EBetP^{X\times Y}} = 3.3723,$$
$$EPDE_{EBetP^{\downarrow X}} + EPDE_{EBetP^{\downarrow Y}} = 2.8833.$$

Therefore, it is clear that $EPDE_{EBetP^{X\times Y}} > EPDE_{EBetP^{\downarrow X}} + EPDE_{EBetP^{\downarrow Y}}$, *thus the subadditivity does not hold.*

Proof: (5) Using the **Example 3**, it has been derived that $EPDE_{EBetP^{X\times Y}} = 3.3723 \neq EPDE_{EBetP^{\downarrow X}} + EPDE_{EBetP^{\downarrow Y}} = 2.8833$. Therefore, the additivity breaks as well. □

C. THE PROPOSED CONFLICT-BASED INFORMATION FUSION PROCESS

By using the proposed Enhanced Pignistic transformation, BPAs are converted into Enhanced Pignistic probabilities, then the Enhanced Pignistic Hellinger Distance can be used to measure the divergence among Enhanced Pignistic probabilities, and the Enhanced Pignistic Deng Entropy can be employed to determine the uncertainty of each *EBetP* functions. When the difference between two sets of *EBetP* functions is larger, the Enhanced Pignistic Hellinger Distance will be larger too. Also, when the volume of uncertain information carried by a piece of *EBetP* function is larger, the Enhanced Pignistic Deng Entropy will be larger as well. Using the definition of EPHD and EPDeng Entropy, from now on, the *EBetP* functions can be exploited for multi-source evidential fusion. A new conflict-based evidential fusion algorithm is proposed as below.

The fusion progress can be separated into the following steps.

Step 1-1 Transform the BPAs into *EBetP* functions via Enhanced Pignistic transformation by using Eq. (9) and (10).

Step 2-1 Construct distance measure matrix *DMM*:

$$DMM = \begin{bmatrix} 0 & EPHD_{1,2} & \cdots & EPHD_{1,N} \\ EPHD_{2,1} & 0 & \cdots & EPHD_{2,N} \\ \vdots & \vdots & \ddots & \vdots \\ EPHD_{N,1} & EPHD_{N,2} & \cdots & 0 \end{bmatrix} \tag{17}$$

where N is the total number of *EBetP* functions.

In line with *DMM*, calculate the average *EPHD* as:

$$\bar{D}_s = \frac{\sum_{r=1, r\neq s}^{N} EPHD_{s,r}}{N-1} \tag{18}$$

where $1 \leqslant s \leqslant N$.

Then calculate the support degree of $EBetP_s$:

$$support_s = \frac{1}{\bar{D}_s} \tag{19}$$

Step 2-2 Since the feasibility of Deng entropy in information fusion has been verified [12], use the EPDeng entropy to measure the uncertainty of $EBetP_s$ through Eq. (15):

$$IDE_s = EPDE_s \tag{20}$$

Then the uncertain information volume of $EBetP_s$ is generated as follows:

$$I_s = e^{IDE_s} \tag{21}$$

Step 3 The evidential weight using the support degree and the information volume is constructed, which is written as:

$$Crd_s = support_s \times I_s \tag{22}$$

Then normalize all these weights and get W_s:

$$W_s = \frac{Crd_s}{\sum_{i=1}^{N} Crd_i} \tag{23}$$

Using the normalized weight, *EBetP* functions are updated as:

$$WEBetP_s = W_s \times EBetP_s \tag{24}$$

The final weighted *EBetP* function is as follows:

$$WEBetP = \sum_{s} WEBetP_s \tag{25}$$

Then fuse the final weighted *EBetP* function through Dempster's combination rule, whose practicality has been proven in **Theorem 1**:

$$FWEBetP = WEBetP \underbrace{\otimes WEBetP \otimes \cdots \otimes}_{N-1 \text{ times}} WEBetP \tag{26}$$

D. NUMERICAL VALIDITY ANALYSIS AND DISCUSSION

The standard checking example involved in **Example 2** is employed for numerical validation and analysis. Fusion results along with seven SOTA (State-of-the-Art) evidential fusion methods are exhibited in Table 2. It is apparent that except Dempster's rule [47], all of the other methods have accurately identified the true class F_1. Note that the newly devised method reached the highest score on the true class F_1 regardless of highly conflicted IS2, which demonstrates the effectiveness of the proposal.

Another strong point of the proposal is it can automatically generate a more reasonable evidential weight on highly conflicted information sources. Table 3 represents the evidential weight generated by the competing algorithms and the proposal on IS2, which carries highly conflicting data. Take

TABLE 2. The identification results of the Example 4. The column index of the bold number corresponds to the identified target of each algorithm.

Algorithm	$\{F_1\}$	$\{F_2\}$	$\{F_3\}$	$\{F_1, F_3\}$	Fault
Dempster's rule [47]	0.0000	0.1422	**0.8578**	0.0000	F_3
Murphy's method [48]	**0.9620**	0.0210	0.0138	0.0032	F_1
Deng's method [49]	**0.9820**	0.0039	0.0107	0.0034	F_1
Yuan's method [50]	**0.9886**	0.0002	0.0072	0.0039	F_1
Xiao's method [11]	**0.9905**	0.0002	0.0061	0.0043	F_1
Zhu's method [6]	**0.9900**	0.0002	0.0052	0.0046	F_1
PSD Pignistic probability [19]	**0.9863**	0.0033	0.0106	0.0034	F_1
Proposed method	**0.9989**	5×10^{-6}	0.0010	6×10^{-5}	F_1

TABLE 3. Evidential weight on IS2 generated by different algorithms.

Algorithm	Evidential weight on IS2
Deng's method [49]	0.0656
Yuan's method [50]	0.0376
Xiao's method [11]	0.0295
Zhu's method [6]	0.0329
PSD Pignistic probability [19]	0.1148
Proposed method	**0.0083**

notice that Dempster's rule [47] and Murphy's method [48] are not evidential weight-based approaches, so they are left out in this analysis. It is clear that the evidential weight on IS2 assigned by the proposed method reaches the lowest among the six involving approaches. It suggests that the proposed fusion framework is more sensitive in identifying high conflict. Comparing with other participated methods, a lower evidential weight is assigned to the highly conflicted information source.

IV. SEMI-AUTOMATIC IMAGE SEGMENTATION WITH CONFLICT-BASED EVIDENTIAL FUSION

In this section, a semi-automatic image segmentation algorithm based on evidential fusion is illustrated. Take notice that current evidence theory-based segmentation methods face two major challenges:

1) The multi-source information conflict in semi-automatic image segmentation is not well managed.
2) The segmentation quality remains uncompetitive comparing with currently advanced algorithms.

Therefore, aims at the two difficulties listed above, this study proposes a course-to-fine approach for semi-automatic segmentation, which can be roughly divided into two stages. Note that since this section, the target hypothesis set becomes $\zeta = 2^{\Theta} = \{\emptyset, \{\text{foreground}\}, \{\text{background}\}, \{\text{unknown}\}\}$, where $\{\text{unknown}\} = \{\text{foreground}\} \cup \{\text{background}\}$, which contains a multi-singleton subset. Thus in the first stage, the proposed fusion algorithm which adopts the Enhanced Pignistic transformation designed in Section III is reasonably applied to tackle information conflict. Two decision-support techniques, named adaptive belief assignment and scalable information extraction, are devised for reasonable BPA generation. In the second stage, fuzzy heuristic refinement is tailored to evidence theory and fuzzy decision-making to improve the segmentation quality. The horizontal workflow of the proposed segmentation approach is shown in Fig. 2.

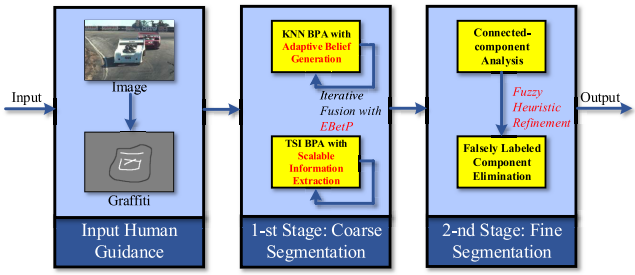

FIGURE 2. The flowchart of the proposed semi-automatic segmentation method.

TABLE 4. Features in feature space.

No.	Feature Description
1	Cartesian coordinates of pixels
2	grayscale values in R, G and B components
3	grayscale values in R, G and B components (after Gaussian filtering)
4	local entropy in R, G and B components

A. THE FIRST STAGE: ADAPTIVE BPA GENERATION AND SCALABLE INFORMATION EXTRACTION

To guarantee segmentation quality, the first stage embraces an iterative segmentation strategy. The number of iterative times is denoted as t, whose initial value is 0. The label matrix is noted as L^i, therefore the initial label matrix is marked as L^0. In this stage, two sources of information are used for pixel classification.

BPA generation is a key factor that affects the decision accuracy [51]. Therefore, adaptively adjusting the belief assigned on uncertainty can model the decision mechanism of a classifier, so as to support the decision made by BPAs and improve the convergence of iterative information fusion. Following this principle, the first uncertain decision-support technique, adaptive belief assignment, is designed to generate the first BPA. First, the K Nearest Neighbors (KNN) classifier is employed to construct the first information source, whose feature space is shown in Table 4. It is trained by user-labeled foreground and background pixels. Then for pixels whose

label is unknown, the probability of being foreground or background is predicted by the KNN classifier, denoted as p_f and p_b respectively.

Through the predicted probability, the first BPA, which is noted as m_{knn}, is formed through Eqs. (27) (which is still in need of normalization):

$$\begin{cases} \bar{m}_{knn}\,(\text{foreground}) = p_f \\ \bar{m}_{knn}\,(\text{background}) = p_b = 1 - p_f \\ \bar{m}_{knn}\,(\text{unknown}) = \dfrac{2}{1 + \exp\{\mu \times \epsilon^t \times d^2\}} \end{cases} \tag{27}$$

where $d = |p_f - p_b|$ measures the difference between p_f and p_b. Here, the parameter μ is used to characterize the belief assigned to "unknown" in the initial time, and the parameter ϵ is devised to adaptively adjust the belief assigned to "unknown" during the iteration, whose value ranges are $(0, +\infty)$ and $(0, 1) \cup (1, +\infty)$ respectively. Take notice that in this task, the belief designated to "unknown" means the belief designated to uncertainty.

Then take a step of normalization and generate m_{knn}:

$$m_{knn}\,(h) = \frac{\bar{m}_{knn}\,(h)}{\sum_l \bar{m}_{knn}\,(l)} \tag{28}$$

where $\sum_l m_{knn}(l) = 1$, and $\forall h, l \in \{\text{foreground, background, unknown}\}$. Therefore, the generation of the first BPA is finished. Theoretical advantages of adopting the adaptive controlling parameters μ and ϵ are stated as below.

- For μ, its supporting influence on adaptively controlling the belief assigned to $\bar{m}_{knn}$ (unknown) has been drawn in Fig. 3. It is clear that when fixing d, the $\bar{m}_{knn}$ (unknown) drops drastically with greater μ. It means that with smaller μ, the unknown pixels are more easily to be identified as foreground or background. Note that μ gives a reasonable impact only on the initial time of decision-making, which is different from ϵ.
- As for ϵ, it offers an effective way to automatically control the belief assignment of KNN BPA as the number of iterations grows. Consider such a circumstance: with the increase of i, the iterative segmentation is still far from convergence. Thus a safe hypothesis, i.e. KNN's decision is getting more incredible, can be made. This issue can be adaptively controlled with the introduction of ϵ, and an example is demonstrated in Table 5. Here suppose $d = 0.2$ and $\mu = 5$, where "$\epsilon = 1.0$" means ϵ has not been introduced. Eq. (27) and Table 5 show that when setting $\epsilon > 1$, as $i \to +\infty$, $\epsilon^i \to +\infty$ is obtained with an exponential growth, which leads to $\bar{m}_{knn}(y^i\,(x_0) = 0) \to 0$. As a result, $\bar{m}_{knn}$(unknown) will rapidly fall. In contrast, when setting $0 < \epsilon < 1$, $\bar{m}_{knn}$(unknown) will adaptively grow.

Note that μ and ϵ offer two strategies on adaptive belief assignment from different perspective, neither of which can be ignored. μ determines how large (or small) the initial uncertainty is, whereas ϵ reflects how fast (or slow) the increasing (or decreasing) of uncertainty is, which keeps running through the iteration process.

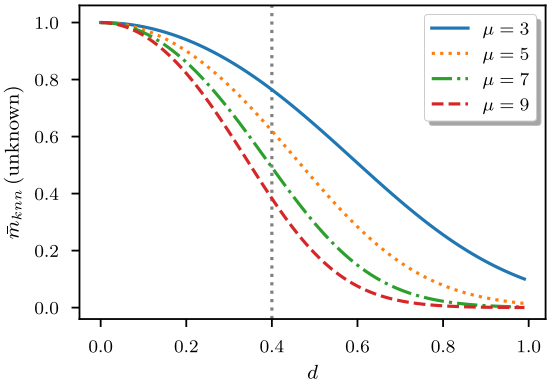

FIGURE 3. The influence of μ on $\bar{m}_{knn}$(unknown).

Spatial information is another important factor that influences segmentation quality [52]. Consequently, introducing a scalable sliding window can help to horizontally capture uncertain information, improve the segmentation consistency in edge areas and accelerate the iterative information fusion. For this reason, the second uncertain decision-support technique, scalable information extraction, is devised to form the second source of information. Considering a rectangle filtering window with size w, for the current unknown pixel at center, the numbers of three types of pixels within the window are marked as $n^i_{foreground}$, $n^i_{background}$ and $n^i_{unknown}$ respectively. Here, the total number of pixels inside the window is defined as N, where $N = w \times w$, and w is the window size. The second BPA, which is named as Tunable-scale Spatial Information BPA (TSI BPA for short), is presented as:

$$m_{tsi}\,(h) = \frac{\exp\left\{\frac{n^i_h}{N}\right\} - 1}{\sum_l \left(\exp\left\{\frac{n^i_l}{N}\right\} - 1\right)} \tag{29}$$

where $h, l \in \{\text{foreground, background, unknown}\}$. The belief assigned on "unknown" indicates the decision probability assigned on uncertainty. Note that TSI BPA contains a changeable parameter w ($N = w \times w$), whose theoretical superiority is stated as behind.

- The TSI BPA stresses a scalable information extraction towards the local spatial distribution of the pixels ready for segmentation. Fig. 5 offers an instance of calculating TSI BPA with $w = 3$ and 7 respectively, and Table 6 uncovers the superiority of changing w. Note that in Table 6, the current pixel is distinguished as "foreground" with $w = 7$, rather than remaining to be "unknown" with $w = 3$. That is because compared with $w = 3$, TSI BPA with $w = 7$ makes better use of spatial information. As a result, a larger w greatly supplements the perception of the central pixel.

TABLE 5. ϵ's adaptively controlling effect on $\bar{m}_{knn}\left(y^i\left(x_0\right)=0\right)$.

$\bar{m}_{knn}$ (unknown)	$i=0$	$i=1$	$i=2$	$i=3$	$i=4$	$i=5$
$\epsilon=0.7$	0.9003	0.9301	0.9510	0.9657	0.9760	0.9832
$\epsilon=1.0$	0.9003	0.9003	0.9003	0.9003	0.9003	0.9003
$\epsilon=1.3$	0.9003	0.8707	0.8325	0.7837	0.7219	0.6449

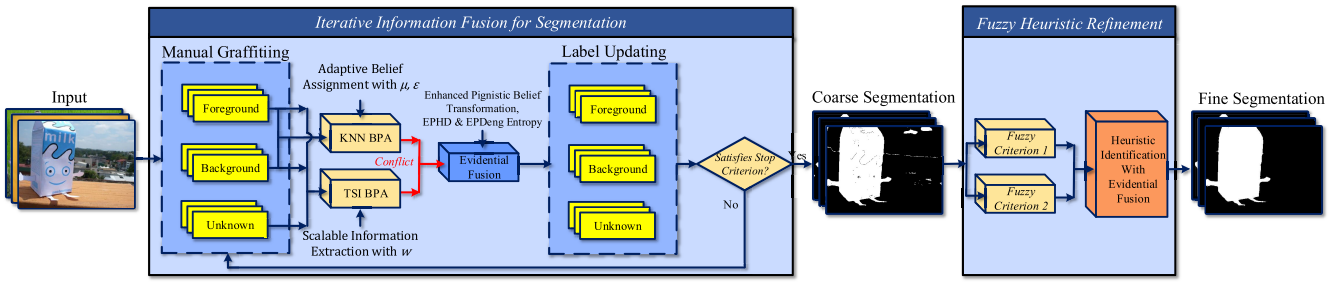

FIGURE 4. Flowchart of the proposed semi-automatic image segmentation method applying evidence theory.

TABLE 6. The BPA results of the central pixel in Fig. 5. With different w, the discriminant results are highlighted bold.

$m_{tsi}(h)$	$w=3$	$w=7$
h =foreground	**0.7213**	0.0965
h =background	0.1893	**0.7722**
h =unknown	0.0894	0.1313

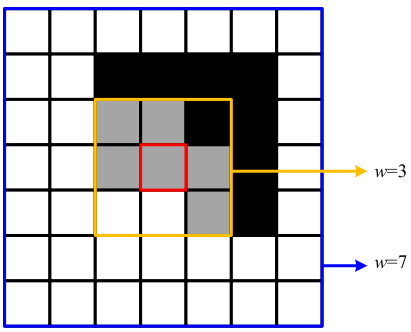

FIGURE 5. An instance of 3 × 3 and 7 × 7 sliding window respectively, the pixel in red rectangle is central pixel. White, black and gray boxes stand for foreground, background and unknown pixels.

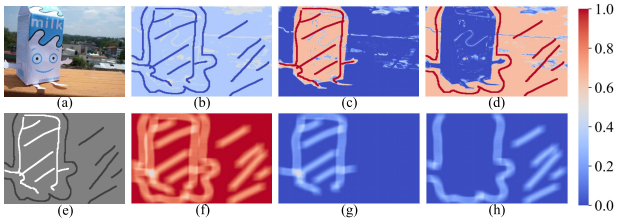

FIGURE 6. The high conflict emerged in our approach, where (a) represents the original image, (b)-(d) are $m_{knn}(h)$, h = {foreground, background, unknown} respectively. (e) is the initial label matrix, and (f)-(h) are $m_{tsi}(h)$, h = {foreground, background, unknown} respectively.

B. THE FIRST STAGE: CONFLICT-BASED EVIDENTIAL FUSION VIA ENHANCED PIGNISTIC PROBABILITY

After the construction of KNN BPA and TSI BPA, their information should be fused. However, it is unfortunate that the information conflict occurs. To explain this problem in image segmentation, the images of m_{knn} and m_{tsi} are exhibited in Fig. 6 respectively. (b)-(d) are the values of m_{knn}, and (f)-(h) are those of m_{tsi} respectively. The deeper red and blue of Fig. 6 represent higher and lower degrees of belief. Then a comparison of (b) and (f), (c) and (g), (d) and (h) in Fig. 6 is made respectively. Note that a significant difference among the three image pairs can be observed: KNN BPA tends to assign a higher belief to "foreground" or "background," whereas TSI BPA assigns more to "unknown." Therefore, it is believed that a high conflict emerges.

To tackle this issue, the conflict-based information fusion algorithm designed in Section III is employed to manage the high conflict. The two conflicting BPAs are firstly converted into $EBetP_{KNN}$ and $EBetP_{TSI}$ functions via Enhanced Pignistic transformation, then fused through the incidental fusion algorithm described in Section III. The flowchart of the fusion process is given in Fig. 7.

Therefore, after the i-th fusion, some unknown pixels are identified as either foreground or background. Consequently, the label matrix changes from L^i to L^{i+1}. In the subsequent iteration, BPAs are regenerated to perform another round of fusion. Also, two stopping criteria are set. One is that the algorithm achieves its maximum number of iterations, and the other is that all of the unknown pixels have been assigned to the target labels ("foreground" or "background"). If the first criterion is met, KNN's prediction is simply assigned to the remained unknown pixels.

C. THE SECOND STAGE: FUZZY HEURISTIC REFINEMENT

In the first stage, adaptive belief assignment, scalable information extraction and highly conflicted evidence have been thoroughly considered. As a result, the proposed method has

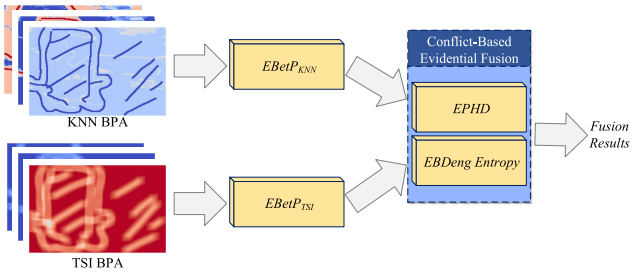

FIGURE 7. The conflict-based fusion process of KNN BPA and TSI BPA.

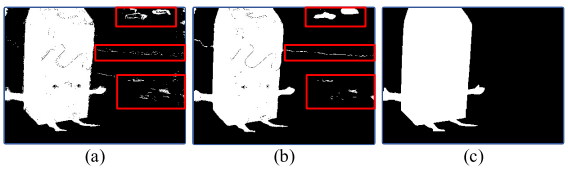

FIGURE 8. An illustration of error propagation, where (a) is the segmentation result solely by KNN, (b) is the result by the first stage of evidential fusion, (c) is Ground Truth.

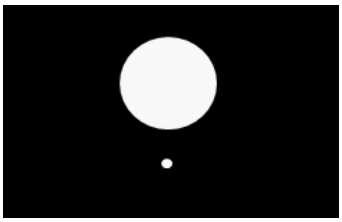

FIGURE 9. An instance of eliminating false foreground: single true foreground component is presented.

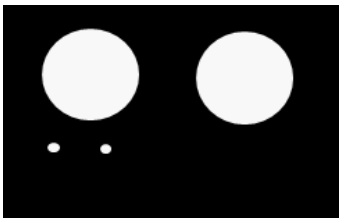

FIGURE 10. An instance of eliminating multiple false foreground: multiple true foreground components are presented.

significant advantages in terms of adaptiveness and decision accuracy. Nonetheless, KNN's erroneous classification is still left out of discussion, which is described as below.

- The negative effect of KNN's erroneous classification is that if, at first, the current pixel's label is wrongly predicted by KNN, false beliefs will be assigned by KNN BPA. Following the iterative fusion, severe error propagation will occur. Error propagation indicates that incorrectly labeled pixels will expand into connected regions and blocks, which seriously harms the segmentation quality. As depicted in Fig. 8, groups of wrongly labeled foreground pixels, which are highlighted by red boxes in (a), have grown into connected blocks in (b).

To deal with this problem, connected-component analysis is used to measure the areas of foreground and background pixel components. From now on, the operation on images is changed from pixel level to connected-component level. Another two sets of BPAs are generated as two fuzzy criteria to make decisions. An fusion-based method is presented to characterize the features of falsely labeled pixel blocks, thus further heuristically find and eliminate them. Note that it is the first attempt to use evidential decision-making to heuristically search and eliminate falsely label pixel components.

Firstly, consider removing false foreground components, and then the false background ones will be handled. Here, false foreground component means the background pixels that have been incorrectly identified as foreground, such as the false foreground boxed in Fig. 8. Note that the area of pixel blocks can be a suitable feature to identify false foreground components. That is because, generally, the number of pixels in a false foreground component is smaller than in a true foreground component. Fig. 9 illustrates this case, in which the circles with a large area and a small area represent the true foreground and the false foreground. Suppose the area of the bigger circle is 100, and that of the smaller circle is 1. The proposal intends to remove the smaller circle.

Assume the area of the current connected-component is S. The total area of foreground components is S_{sum}. It can be observed that one component is more likely to be a false foreground component if S is smaller. Thus, a higher degree of belief should be assigned to background. According to this principle, the first evidence, which serves as the first fuzzy decision-making criteria, is given below:

$$\begin{cases} \bar{m}_1\,(\text{foreground}) = \frac{S}{S_{sum}} \\ \bar{m}_1\,(\text{background}) = 1 - \frac{S}{S_{sum}} = 1 - \bar{m}_1\,(\text{foreground}) \\ \bar{m}_1\,(\text{unknown}) = \exp\{-|\bar{m}_1\,(\text{foreground}) \\ \qquad\qquad\qquad - \bar{m}_1\,(\text{background})\,|\} \end{cases} \tag{30}$$

The BPA in Eq. (30) is then normalized as follows:

$$m_1\,(h) = \frac{\bar{m}_1\,(h)}{\sum_l \bar{m}_1\,(l)} \tag{31}$$

where $h, l \in \{\text{foreground, background, unknown}\}$. After normalization, this BPA satisfies $\sum_h m_1\,(h) = 1$, and it will be used for the subsequent decision-making. If the current connected-component is classified as "foreground" using m_1, its label will be set as foreground. Otherwise, if it is identified as "background," its label will be reset to background. Besides, the label may remain "unknown" as the third outcome, if the connected pixel block is distinguished as "unknown" and there is no strong evidence to indicate a target category, thus its current label will be remained. The management of background can be treated after a reverse operation on the binary output.

Here, the instance represented in Fig. 9 is still used to illustrate the decision-making process. The BPA of

the smaller circle, which is obtained from Eqs. (30) and (31), is m_1 (foreground) $= 0.0072$, m_1 (background) $= 0.7199$, m_1 (unknown) $= 0.2729$. It is clear that m_1 (foreground) $< m_1$ (unknown) $< m_1$ (background). Thus this connected-component is classified as background. The label of the smaller circle is then set to be background, which means that the false foreground component is successfully corrected.

However, it is noticed that the single BPA m_1 cannot explicitly deal with the scenario where the true foreground is divided into several connected-components. This shortcoming can be briefly illustrated using an example in Fig. 10, where the two bigger circles at the top are the true foreground, while the two smaller circles at the bottom are the false foreground. We intend to eliminate the two smaller circles.

Suppose the areas of the two bigger circles are both 100, and those of the smaller circles are 1. Using the first BPA on smaller circles, m_1 (foreground) $= 0.2487$, m_1 (background) $= 0.2537$, m_1 (unknown) $= 0.4926$. Clearly m_1 (foreground) $<$ m_1 (background) $<$ m_1 (unknown) is achieved. Thus, the classification result is ''unknown'', which indicates this BPA fails to detect the true background component. As a result, a second BPA is needed to support making more accurate decisions. As a result, suppose S_{max} and S_{min} are the largest and smallest areas among all true and false foreground components. Then the second BPA, which serves as the second fuzzy decision-making criteria, is built as Eqs. (32):

$$\begin{cases} \bar{m}_2\,(\text{foreground}) = \dfrac{S}{S_{max}} \\ \bar{m}_2\,(\text{background}) = \dfrac{S_{min}}{S} \\ \bar{m}_2\,(\text{unknown}) = \exp\{-|\bar{m}_2\,(\text{foreground}) - \bar{m}_2\,(\text{background})\,|\} \end{cases} \tag{32}$$

Then the BPA is normalized as below:

$$m_2\,(h) = \frac{\bar{m}_2\,(h)}{\sum_l \bar{m}_2\,(l)} \tag{33}$$

where $h, l \in \{\text{foreground}\}$, and $\sum_l m_2\,(l) = 1$. After this procedure, the two sets of BPAs are fused by the Dempster's combination rule. The fusion result of the instance in Fig. 10 is m_2 (foreground) $= 0.0072$, m_2 (background $= 2$) $= 0.7238$, m_2 (unknown) $= 0.2690$, which indicates $\bar{m}_2$ (foreground) $<$ $\bar{m}_2$ (unknown) $<$ $\bar{m}_2$ (background). Thus despite the confused m_1, by using Dempser's combination rule [30], the label of small circles is still rectified to be background, and the false foreground component is successfully removed.

In Fig. 11, an exemplary illustration towards the two BPAs is drawn to numerically analyze the effect of the two fuzzy criteria on decision-making and further uncover the feasibility of the proposed refinement structure. In this instance, $S_{max} = 100$, $S_{min} = 1$, $S_{sum} = 200$. Note that with the area of the pixel block increasing, i.e. with S raising, the decision made by m_1 will gradually vary from ''background'' to ''unknown'', then finally becomes ''foreground''. It means the larger the pixel component is, the more likely it should be a component of true foreground, which is reasonable. As for m_2, the larger the component is, the likelihood of it being a true background component is smaller. Thus, less belief is assigned to background, and consequently more beliefs are simultaneously designated to foreground and unknown. Then from the perspective of decision-making, it is interesting that when the area of pixel components is less than 31, this component will be directly decided to be background since the two BPAs have given the same decisions. When the area of this component is from 31 to 69, the criteria m_1 will be confused, thus it will make the decision ''unknown''. However, due to the reason that larger belief has been assigned to ''background'' by m_2, then the component can still be identified as ''background''. Only when the area is larger than 69, high conflict will emerge between the two criteria, thus the decision will be uncertain. By using this example, the practicability of the proposed refinement algorithm can be verified theoretically.

Moreover, to further clarify the feasibility of the proposed fuzzy heuristic refinement algorithm from an experimental perspective, the result after refinement of Fig. 8 (b) is shown in Fig. 13. In contrast to Fig. 13 (a), no false foreground and false background are observed in Fig. 13 (b). Consequently, it strongly suggests the simple but useful proposal embedded in the second stage further improves the quality of image segmentation significantly. Fig. 4 demonstrates the full flowchart of the proposed semi-automatic image segmentation algorithm which employing evidence theory in detail.

V. EXPERIMENTAL ANALYSIS

This section focuses on the experimental analysis to specify the performance of the proposed segmentation method. Analysis and discussions on the advantages of the embedded information fusion model, adaptive belief assignment, scalable information extraction and fuzzy heuristic refinement proposed in this paper are also included.

A. DATASETS PREPARATION

In order to comprehensively investigate the performance of algorithms, two standard checking datasets, i.e. Grabcut [53] dataset and ECCSD [54] dataset, are chosen in this section. The two datasets comprise 50 and 1000 images, respectively, for a standard semi-automatic segmentation test.

B. STATE-OF-THE-ART ALGORITHMS FOR COMPARISON AND IMPLEMENTATION DETAILS

Seven state-of-the-art semi-automatic image segmentation algorithms (including the proposed one) have been involved in the experiment, which are DS [28], SMRW [55], RaWaCs [56], LC [57], LPCN [58] and IOG-ResNet101 [59]. Note that DS [27] is one of the only two semi-automatic image segmentation methods in connection with evidence theory, which is mainly studied in this paper. The other

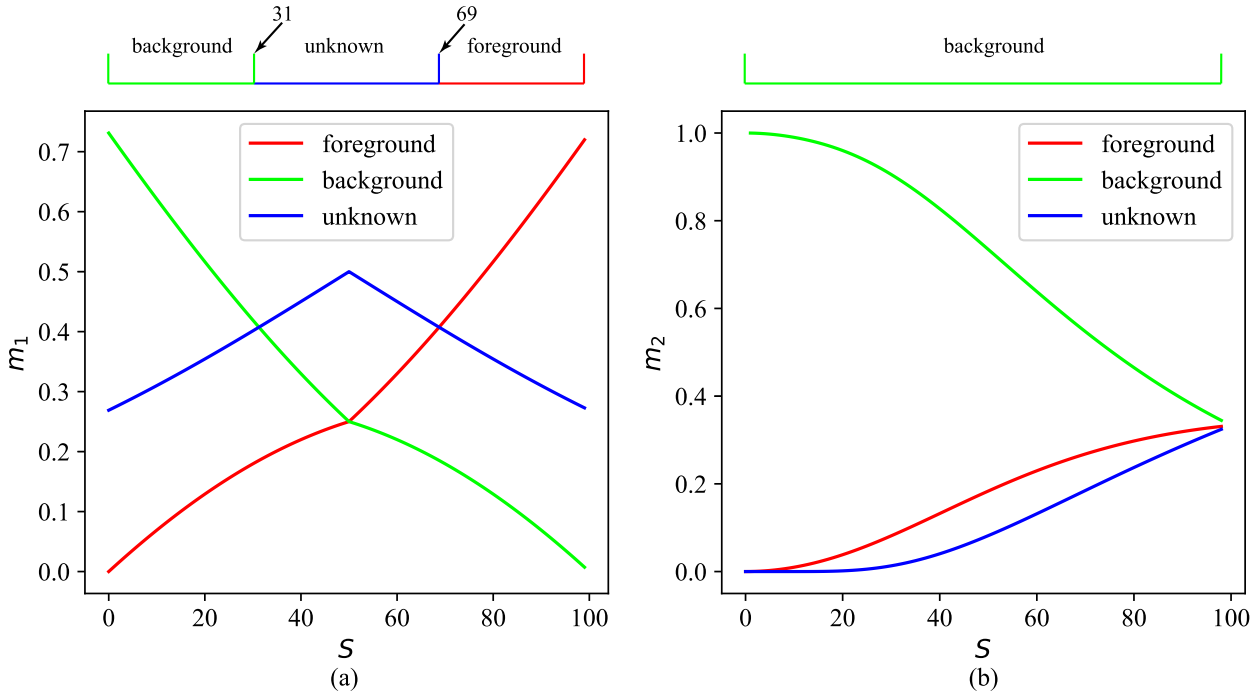

FIGURE 11. A numerical illustration of the two fuzzy BPAs set for heuristic enhancement, where (a) is the relation between m_1 and S, (b) is the relation between m_2 and S. In this example, $S_{max} = 100$, $S_{min} = 1$ and $S_{sum} = 200$ are set.

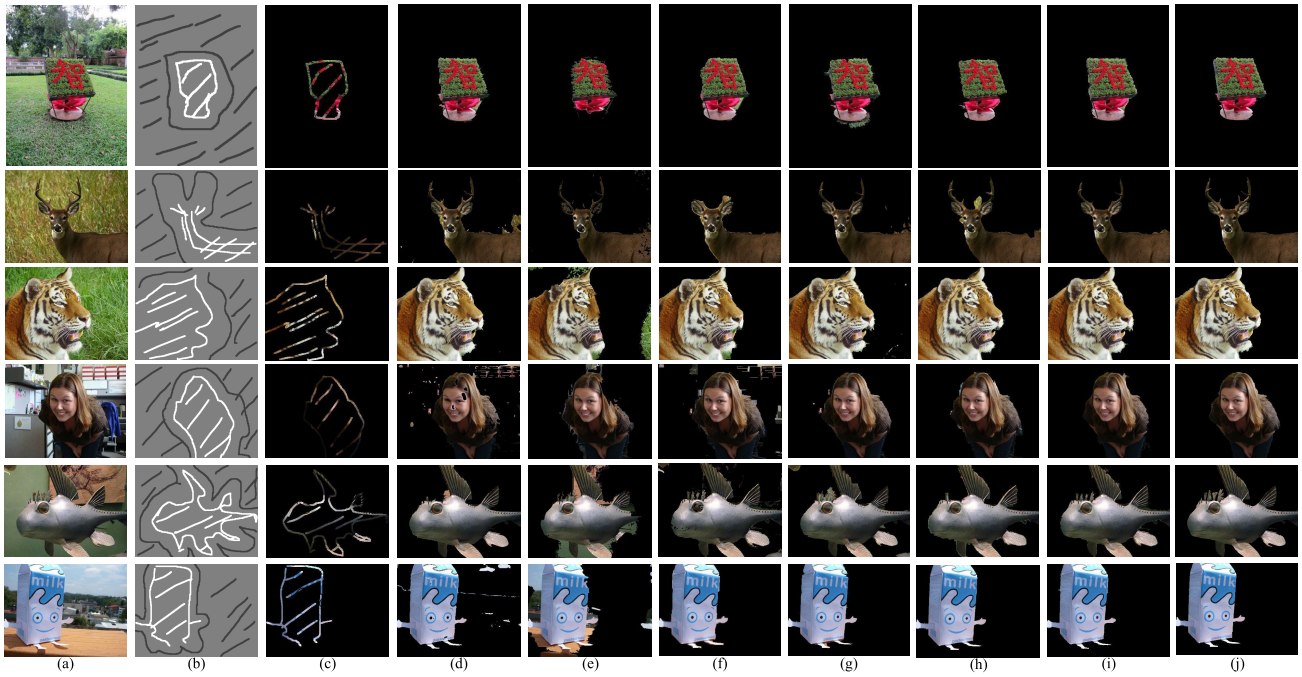

FIGURE 12. Superiority analysis: Segmentation results on Grabcut dataset [53]. The representation of each column is as follows: (a) original image, (b) initial labeling, (c) DS [28], (d) SMRW [55], (e) RaWaCs [56], (f) LC [57], (g) LPCN [58], (h) IOG-ResNet101 [59], (i) proposed method and (j) Ground Truth.

one, [27], is so computationally consuming that we cannot gain any output from this method on our experimental platform. However, as verified in [27], this method works worse than Grabcut [53], which lacks superiority compared with LPCN [58].

Algorithms are tested on an Intel I5-7200U CPU, 4.00 GB RAM platform. The proposed algorithm is developed on Python 3.7, and MATLAB image labeler is used for interactive labeling. As for the parameters in the first stage of evidential fusion, $\mu = 3$, $\epsilon = 0.95$ and $w = 11$ are set.

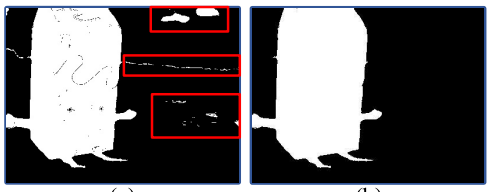

FIGURE 13. Segmentation refinement of Fig. 8, where (a) is segmentation result after the first stage of evidential fusion, as have depicted in Fig. 8(b), while (b) is the refined output after the second stage of evidential fusion.

C. QUANTITATIVE EVALUATION CRITERIA

In this paper, Accuracy (Acc), mean Intersection-over-Union (mIoU), Dice coefficient (Dice) and F-measure are adopted to comprehensively compare the performance of algorithms. The four criteria are introduced as follows [60]:

$$Acc = \frac{TN + TP}{TN + TP + FN + FP} \tag{34}$$

$$mIoU = \frac{\sum_k IoU_k}{2} \tag{35}$$

$$Dice = \frac{2 \times TP}{2 \times TP + FP + FN} \tag{36}$$

$$F - measure = \frac{1 + \beta^2 \times Pre \times Rec}{\beta^2 \times Pre + Rec} \tag{37}$$

where $IoU_k = \frac{TP}{TP+FP+FN}$ for each label k (in this study, the target labels are foreground and background), $Pre = \frac{TP}{TP+FP}$ and $Rec = \frac{TP}{TP+FN}$. TP and TN are the correctly segmented foreground and background pixels. FN denotes background pixels wrongly segmented as foreground, while FP indicates foreground pixels wrongly segmented as background. In this study, β is set to 1, thus the F-measure is equivalent to F1-score [61].

D. COMPARATIVE AND SUPERIORITY ANALYSIS

In this section, the segmentation results from competing algorithms are visualized, and their performances are quantitatively evaluated and analyzed. Fig. 12 and Fig. 14 depict the original images, initial labeling, and segmentation results of ECSSD [54] and Grabcut [53] datasets respectively.

From Fig. 12 and Fig. 14, it is clear that DS [28], which also employs evidence theory, yields the worst segmentation results, as only manually marked foreground is detected. That is because the pixel feature extraction in DS [28] algorithm is too naive to handle images with complex content. In addition, it is found that RaWaCs [56] and SMRW [55] are susceptible to oversegmentation. Edges and corners are not appropriately segmented in their outputs. The explanations for the oversegmentation of RaWaCs [56] and SMRW [55] are similar. Due to the Random Walk [62] base algorithm embedded in RaWaCs [56] and SMRW [55], the edge pixels are sensitive to the pixel distance in their pre-fixed color space. As for IOG-ResNet101 [59], it faces an oversegmentation more slightly. The oversegmentation of IOG-ResNet101 [59] is it sometimes cannot distinguish the background pixels through input features, especially when the features of different kinds of pixels are close to foreground pixels regardless of their refined network structure. On the contrary, LC [57] and LPCN [58] can generate more stable results. That is because the mathematical formulation in LC [57] has an anisotropic behavior, thus the image details are fitted better. For LPCN [58], it uses a complex network to repeatedly improve the segmentation accuracy. However, some wrongly segmented pixel blocks at the boundaries of entities and scenes, or some falsely segmented foreground regions inside background can still be observed. It is noticeable that the proposed algorithm outperforms these competing algorithms, with edge areas and details of objects segmented more accurately. What is more, no large incorrectly labeled pixel blocks can be observed, which demonstrates the robustness of the proposal.

Quantitative analysis in terms of the four criteria are summarized in Table 7 and Table 8, which are analyzed on ECSSD [54] and Grabcut [53], respectively. It is clear that in the two tables, the proposed method outperforms the competing methods with major comprehensiveness, which ranks first under all four objective criteria. It provides strong evidence to reveal the validity and superiority of the proposed segmentation algorithm.

E. ABLATION STUDY AND ANALYSIS

This section intends to uncover the advantage of applying 1) the devised Enhanced Pignistic transformation-based fusion algorithm in semi-automatic image segmentation, and 2) the heuristic refinement which firstly embraces evidential fuzzy decision-making. Fig. 16 compares the segmentation quality of each stage's fusion from an objective perspective, where four evaluation criteria are adopted for validation. In this comparison, "Without Fusion" means no information fusion is used, i.e. the segmentation result is only based on KNN BPA and TSI BPA. "1-st Stage Fusion Only" refers to the result using the conflict-based iterative evidential fusion algorithm with proposed conflict-based evidential fusion incorporating Enhanced Pignistic transformation, regardless of the proposed heuristic fuzzy refinement. "Proposed" indicates the result using the proposed method with two stages of fusion. Fig. 17 visualizes the segmentation results under these three circumstances.

According to Fig. 17, the segmentation output in the case of "1-st Stage Fusion Only" is more consistent than that of "Without Fusion." And the falsely labeled pixels are even less in the case of "Proposed" than that of "1-st Stage Fusion Only", thus the segmentation quality get better and better from no fusion involved to the proposed method. This interesting finding strongly confirms that a better segmentation is associated with adopting the Enhanced Pignistic transformation in semi-automatic image segmentation, and the proposed heuristic refinement also contributes to segmentation quality improvement. The same conclusion can be drawn from Fig. 16. Comparing the cases of "Without

FIGURE 14. Superiority analysis: Segmentation results on ECSSD dataset [54]. The representation of each column is as follows: (a) original image, (b) initial labeling, (c) DS [28], (d) SMRW [55], (e) RaWaCs [56], (f) LC [57], (g) LPCN [58], (h) IOG-ResNet101 [59], (i) proposed method and (j) Ground Truth.

TABLE 7. Superiority analysis: Performance of state-of-the-art algorithms on ECCSD [54] dataset.

Method	Acc	mIoU	Dice	F-measure
DS [28]	0.749(±0.230)	0.447(±0.229)	0.273(±0.140)	0.436(±0.084)
SMRW [55]	0.964(±0.064)	0.907(±0.018)	0.925(±0.026)	0.900(±0.100)
RaWaCs [56]	0.928(±0.049)	0.828(±0.131)	0.857(±0.125)	0.866(±0.087)
LC [57]	0.967(±0.063)	0.912(±0.061)	0.932(±0.054)	0.942(±0.052)
LPCN [58]	0.974(±0.016)	0.923(±0.042)	0.944(±0.033)	0.942(±0.033)
IOG-ResNet101 [59]	0.970(±0.014)	0.927(±0.050)	0.944(±0.049)	0.944(± 0.050)
Proposed method	**0.975(±0.012)**	**0.932(±0.033)**	**0.948(±0.144)**	**0.945(±0.032)**

TABLE 8. Superiority analysis: Performance of state-of-the-art algorithms on Grabcut [53] dataset.

Method	Acc	mIoU	Dice	F-measure
DS [28]	0.832(±0.103)	0.497(±0.135)	0.294(±0.159)	0.411(±0.135)
SMRW [55]	0.854(±0.131)	0.757(±0.138)	0.764(±0.119)	0.734(±0.204)
RaWaCs [56]	0.820(±0.135)	0.690(±0.224)	0.697(±0.193)	0.678(±0.170)
LC [57]	0.957(±0.053)	0.863(±0.097)	0.904(±0.105)	0.896(±0.144)
LPCN [58]	0.958(±0.022)	0.915(±0.079)	0.899(±0.093)	0.901(±0.145)
IOG-ResNet101 [59]	0.960(±0.019)	0.918(±0.030)	0.904(±0.032)	0.908(±0.148)
Proposed method	**0.962(±0.034)**	**0.920(±0.022)**	**0.907(±0.043)**	**0.910(±0.145)**

Fusion'' with ''1-st Stage Fusion Only'' in Fig. 16, it can be clearly seen that the conflict-based iterative evidential fusion algorithm has successfully improved the segmentation quality, where the new *EBetP* functions, Enhanced Pignistic Hellinger Distance and Enhanced Pignistic Deng Entropy are proposed and applied in semiautomatic segmentation. The comparison between the cases of ''1-st Stage Fusion Only'' and ''Proposed'' reveals that the second stage of segmentation

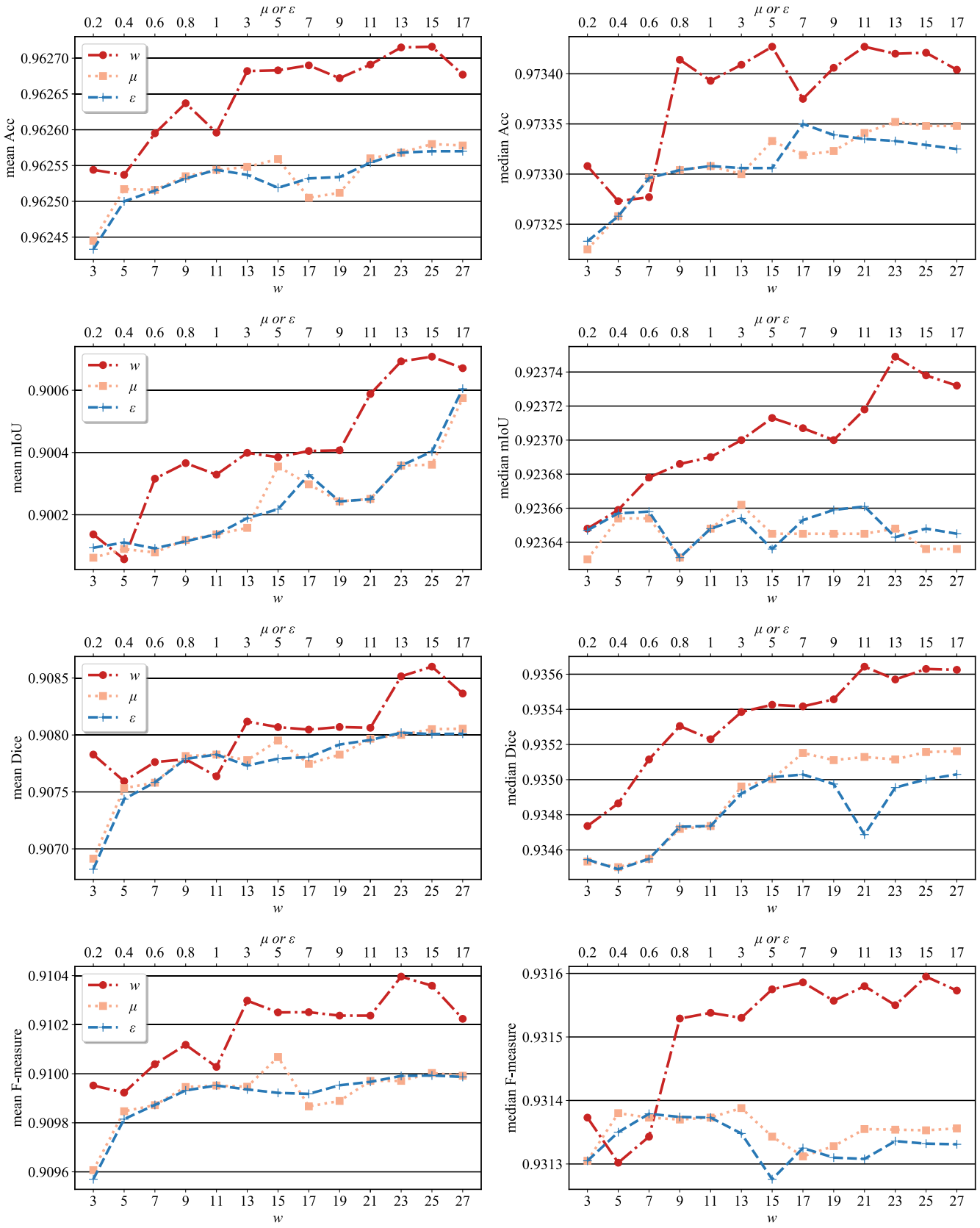

FIGURE 15. Sensitivity analysis: Mean and median Acc, mIoU, Dice and F-measure with different w, μ and ϵ.

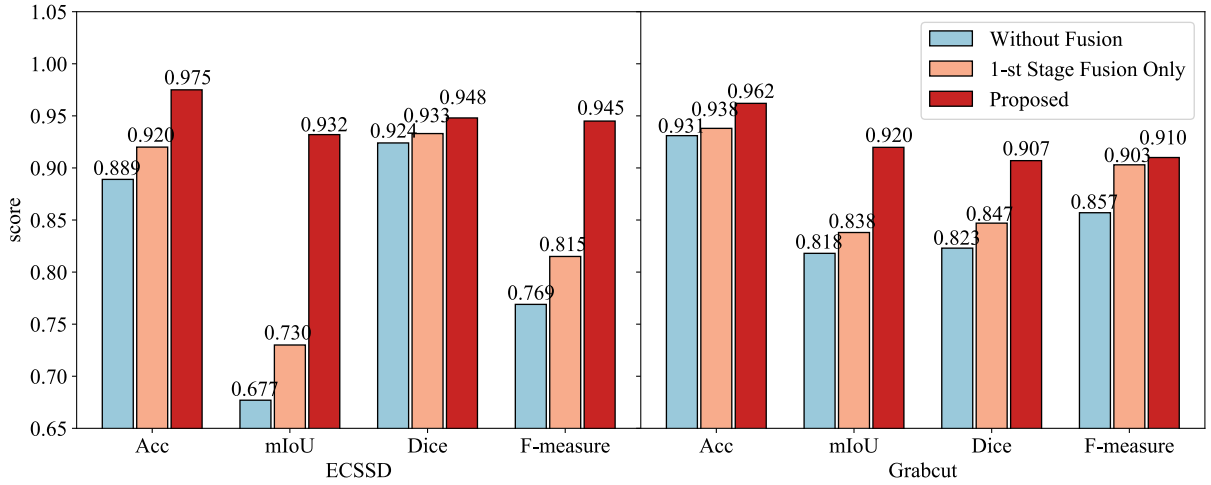

FIGURE 16. Ablation study: Performance improvement of each stage of evidential fusion. The ordinate is the score of each criterion.

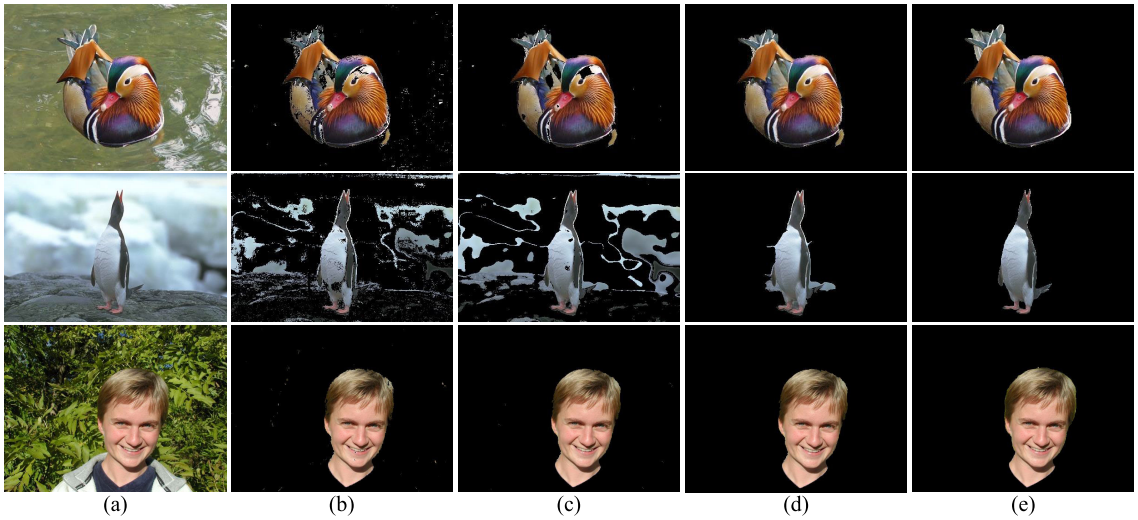

FIGURE 17. Ablation study: The segmentation results under conditions (b) "Without Fusion", (c) "1-st Stage Fusion Only" and (d) "Proposed". Here, (a) is the original image and (e) is Ground Truth.

has further improved results under four criteria, which helps to achieve the best segmentation results. Note that without the second stage of evidential fusion, the proposal is not competitive with most of the involved SOTA algorithms, which manifests the efficiency of proposing the evidential heuristic refinement. This result also broadly supports the view that the two stages of information fusion can improve segmentation results independently. At first, the Enhanced Pignistic transformation-based fusion offers a relatively good benchmark for segmentation performance, while the following fuzzy heuristic refinement significantly improves the segmentation quality.

F. TIME COMPLEXITY ANALYSIS

This section focuses on time complexity analysis. To start with, suppose the image size is $h \times w$. In the first stage, the time complexity of KNN classifier is $O((h \times w)^2)$, and the time complexity to capture spatial information is $O(h \times w)$. Suppose the maximum iteration number is M, then the time complexity of the first stage is $O(M \times (h \times w)^2)$. In the second stage, denote the number of pixel components is C, thus the time complexity of this stage is $O(C)$. Therefore, the total time complexity is $O(M \times (h \times w)^2 + C)$.

G. KEY PARAMETERS ANALYSIS AND DISCUSSION

In this section, experiments are contained to discuss the two practical advantages of the adaptive belief assignment and scalable information extraction. Note that their theoretical advantages have been discussed in Section IV-A at full length. Grabcut dataset [53] is employed to analyze the influence of the three key parameters involved in the two decision-support techniques, thus further demonstrating how they affect the performance of the proposal. Parameters' default values are $\mu = 1$, $\epsilon = 1$ and $w = 3$. To make a fare comparison, when

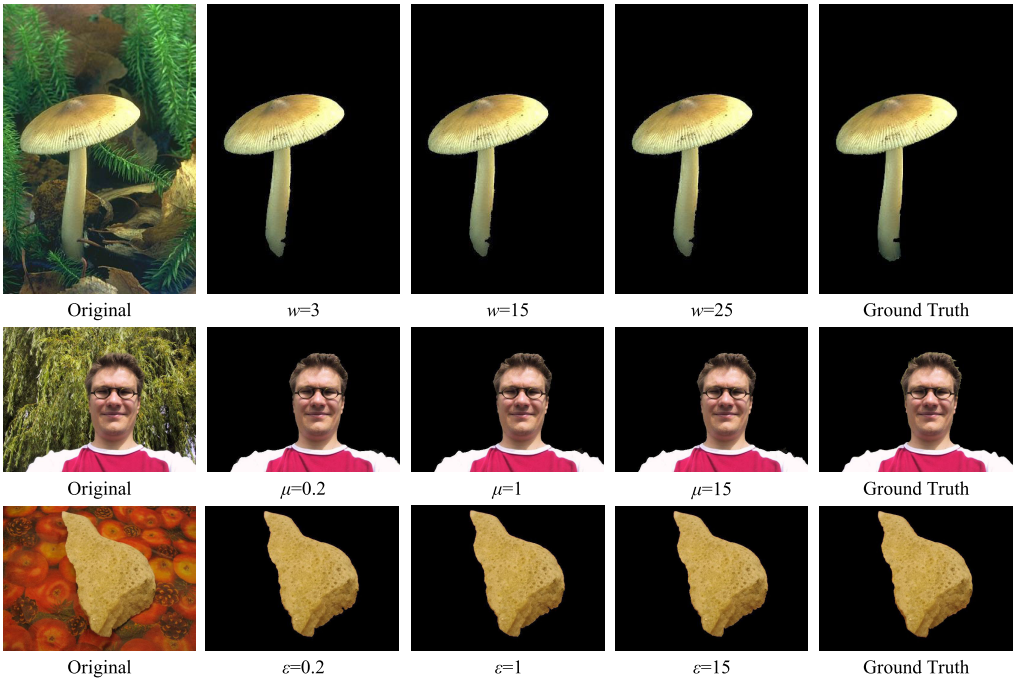

FIGURE 18. Sensitivity analysis: The segmentation results with different parameters.

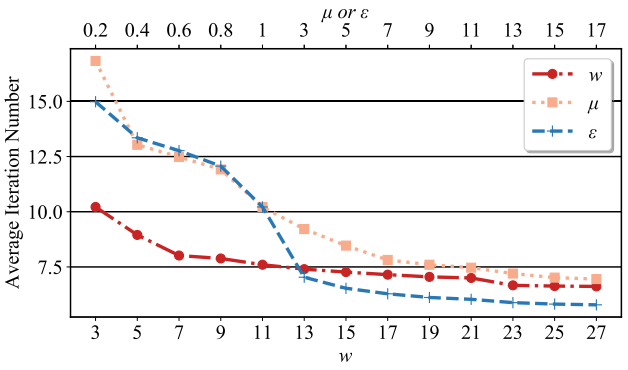

FIGURE 19. Iteration convergence analysis: The average iteration number with changing w, μ and ϵ.

any of the three parameters is studied, the other two remain the default.

1) ITERATION CONVERGENCE ANALYSIS AND DISCUSSION

Studying the iteration number in the first stage of the proposal can unfold the accelerating property of changing parameters, which is the first practical advantage. The curves of the average iteration number with three parameters are shown in Fig. 19. It is surprising that the three curves all drop in the same pattern, manifesting that larger values of the three parameters can accelerate the iteration convergence, especially in contrast with their respective default values. However, the underlying reasons are slightly different, which needs further discussion.

Firstly, the downward trend of μ and ϵ can be explained by the adaptive BPA generation principle. According to Eqs. (27), when d is a constant, a larger μ brings about a lower volume of uncertain information. The finding in Fig. 19 implies that a lower degree of decision uncertainty favors faster decision-making. As for ϵ, when $\epsilon > 1$, the degree of decision uncertainty decays swiftly. Thus the proposed method tends to immediately segment unknown pixels into foreground or background. The opposite condition, i.e. the condition with $0 < \epsilon < 1$ can be analyzed similarly. Another interesting conclusion is that the curve of ϵ declines slightly sharper than μ when they are both greater than 1, which proves that ϵ more significantly impacts the acceleration of the iteration convergence. It can be explained that ϵ is a parameter that controls the belief assigned on uncertain throughout the iteration process, while μ is a parameter that only determines the initial uncertainty belief.

Secondly, the steady drop of w can be explained by the intrinsic property of scalable information extraction. When the labeled pixels are far less than the unknown, more unknown pixels can be covered by a larger window size w. A higher volume of uncertain information is thus given by TSI BPA. Decision-making mainly relies on KNN BPA in initial times of the following evidential fusion, with more unknown pixels being directly assigned as foreground or background. It makes our algorithm converge fast. As the number of iterations increases, the number of foreground and background pixels gradually increases. When more labeled pixels enter the receptive field, the degree of uncertainty

gets lower, which in turn aids the iterative decision-making process to terminate earlier.

2) SENSITIVITY ANALYSIS AND DISCUSSION

Sensitivity analysis reveals the proposal's balance between robustness and high performance, which is the second practical advantage of the two proposed uncertain decision-support techniques. Also, the best region of parameters can also be determined. Here, the segmentation results can be seen in Fig. 18. The mean and median values of the four involved metrics, which are Acc, mIoU, Dice and F-measure, are used for systematical sensitivity investigation, where the test results are displayed in Fig. 15.

As can be observed from Fig. 18, the segmentation results are visually stable and robust to changed parameters, suggesting the robustness of the two proposed decision-support techniques. That is because most of falsely segmented pixels have been removed in the fuzzy heuristic refinement stage. By analyzing Fig. 18, it also indicates that the changed parameters can affect the segmentation quality of edge areas. It suggests that the higher the three parameters are, the segmented images' edge and corners are more consistent and maintained. Partially consistent with the finding aforementioned from the visual analysis, a further conclusion can also be drawn by analyzing the numerical curves in Fig. 15. For the parameters μ and ϵ, in spite of median mIoU and median F-measure showing a fluctuated trend, the larger the two parameters are, the other six metrics get higher scores, implying the segmentation process works better. That can be explained that with the decision uncertainty decreasing, the decision accuracy gradually raises correspondingly. As for the parameter w, the scores on the eight metrics increase before it exceeds 23. It reflects such a phenomenon: the larger w is, the better the proposal works. However, when the parameter w is greater than 23, the mean F-measure begins to drop. And when the parameter w is greater than 25, a clear downtrend on the remaining metrics except median F-measure (which only shows significant fluctuation when the parameter w is at around 25) can also be observed. In other words, the performance of proposal may be getting worse if the parameter w is greater than 25. Such a downward trend can be explained that the sliding window is getting too large for spatial information extraction, therefore, the decision made by TSI BPA becomes imprecise. Note that the outcome of sensitivity analysis not only verifies the robustness of the two proposed decision-support techniques, but also provides guidance for further parameter fine-tuning in real-world applications.

VI. CONCLUSION

Current Pignisic probability generation scheme has shortcomings in managing the loss of information. Recent evidence theory-based semi-automatic segmentation methods also confront information conflict and lack robust decision accuracy. Therefore, this paper mainly proposes Enhanced Pignistic transformation with a novel conflict-based evidential fusion algorithm, as well as a new semi-automatic image segmentation approach that adopts evidential information fusion and decision-support techniques.

In the study of Pignistic transformation, its limitation on probability degeneration of the *BetP* function is uncovered, and the Enhanced Pignistic transformation is devised to tackle this problem. Later, the definition of Enhanced Pignistic Hellinger Distance and Enhanced Pignistic Deng Entropy are proposed with their properties proved. Then a new information fusion framework is established and validated via a case study, uncovering its superiority in decision-making and evidential weight generation.

Then the Enhanced Pignistic transformation-based information fusion scheme is embedded into the proposed segmentation approach to tackle the information conflict. To further improve the segmentation quality, adaptive belief generation and scalable information extraction are designed for uncertain decision support. Moreover, heuristic refinement firstly incorporating evidence theory and fuzzy decision-making is also proposed for segmentation enhancement. Experimental results show several empirical findings. First, the proposal outperforms six competing algorithms on four metrics each. Besides, in the ablation study, the advantage of incorporating Enhanced Pignistic transformation-based fusion and heuristic refinement is uncovered. Time complexity has also been discussed and analyzed. Moreover, two practical merits of adaptive belief assignment and scalable information extraction are also discussed in the iteration analysis and the sensitivity test. It is suggested that with the three key parameters increasing, the iteration for convergence gets faster. But it is also found that they draw subtly different impacts on the four criteria in image segmentation.

Note that the proposed Enhanced Pignistic transformation is only tested and applied in the task of semi-automatic image segmentation. Also, as pointed out by Moral-García [45], we must admit the Deng entropy itself and its refined entropies still have challenges but remaining unsolved by researchers. In further studies, we will try to combine the proposed belief reassigning structure with more real world problems to expand its applications, and try to produce more inspiring works on justifying reasonable entropies in evidence theory.

REFERENCES

[1] Y. Zhang, Q. Xiao, X. Deng, and W. Jiang, "A multi-source information fusion method for ship target recognition based on Bayesian inference and evidence theory," *J. Intell. Fuzzy Syst.*, vol. 42, no. 3, pp. 2331–2346, Feb. 2022.

[2] S. Zhang and F. Xiao, "A TFN-based uncertainty modeling method in complex evidence theory for decision making," *Inf. Sci.*, vol. 619, pp. 193–207, Jan. 2023.

[3] Y. Liu and Y. Tang, "Managing uncertainty of expert's assessment in FMEA with the belief divergence measure," *Sci. Rep.*, vol. 12, no. 1, p. 6812, Apr. 2022.

[4] R. Li, Z. Chen, H. Li, and Y. Tang, "A new distance-based total uncertainty measure in Dempster–Shafer evidence theory," *Appl. Intell.*, vol. 52, no. 2, pp. 1209–1237, Jan. 2022.

[5] W. Fan and F. Xiao, "A complex Jensen–Shannon divergence in complex evidence theory with its application in multi-source information fusion," *Eng. Appl. Artif. Intell.*, vol. 116, Nov. 2022, Art. no. 105362.

[6] C. Zhu and F. Xiao, "A belief Hellinger distance for D–S evidence theory and its application in pattern recognition," *Eng. Appl. Artif. Intell.*, vol. 106, Nov. 2021, Art. no. 104452.
[7] Y. Tang, Y. Chen, and D. Zhou, "Measuring uncertainty in the negation evidence for multi-source information fusion," *Entropy*, vol. 24, no. 11, p. 1596, Nov. 2022.
[8] Y. Tang, S. Tan, and D. Zhou, "An improved failure mode and effects analysis method using belief Jensen–Shannon divergence and entropy measure in the evidence theory," *Arabian J. Sci. Eng.*, vol. 47, pp. 1–14, Dec. 2022.
[9] C. Zhu, B. Qin, F. Xiao, Z. Cao, and H. M. Pandey, "A fuzzy preference-based Dempster–Shafer evidence theory for decision fusion," *Inf. Sci.*, vol. 570, pp. 306–322, Sep. 2021.
[10] A.-L. Jousselme, D. Grenier, and É. Bossé, "A new distance between two bodies of evidence," *Inf. Fusion*, vol. 2, no. 2, pp. 91–101, Jun. 2001.
[11] F. Xiao, "Multi-sensor data fusion based on the belief divergence measure of evidences and the belief entropy," *Inf. Fusion*, vol. 46, pp. 23–32, Mar. 2019.
[12] C. Zhu, F. Xiao, and Z. Cao, "A generalized Rényi divergence for multi-source information fusion with its application in EEG data analysis," *Inf. Sci.*, vol. 605, pp. 225–243, Aug. 2022.
[13] Z. Deng and J. Wang, "A novel decision probability transformation method based on belief interval," *Knowl.-Based Syst.*, vol. 208, Nov. 2020, Art. no. 106427.
[14] M. Song, C. Sun, D. Cai, S. Hong, and H. Li, "Classifying vaguely labeled data based on evidential fusion," *Inf. Sci.*, vol. 583, pp. 159–173, Jan. 2022.
[15] H. M. Kamdjou, E. T. Fute, A. E. Amraoui, and A. Nzeukou, "The transferable belief model for failure prediction in wireless sensor networks," *Social Netw. Comput. Sci.*, vol. 2, no. 4, p. 269, Jul. 2021.
[16] A. Derder, L. Khelladi, and Z. Doukha, "A prediction-based protocol for online target tracking in VSNs," *Telecommun. Syst.*, vol. 78, no. 3, pp. 377–389, Nov. 2022.
[17] L. Jiao, T. Denæux, Z.-G. Liu, and Q. Pan, "EGMM: An evidential version of the Gaussian mixture model for clustering," *Appl. Soft Comput.*, vol. 129, Nov. 2022, Art. no. 109619.
[18] Q. Zhang, H. Li, R. Li, and Y. Tang, "An improved measure for belief structure in the evidence theory," *PeerJ Comput. Sci.*, vol. 7, Sep. 2021, Art. no. e710.
[19] J. Zhu, X. Wang, and Y. Song, "A new distance between BPAs based on the power-set-distribution pignistic probability function," *Appl. Intell.*, vol. 48, no. 1, pp. 1506–1518, Jun. 2018.
[20] L. Martin and J. Sudano, "Yet another paradigm illustrating evidence fusion (YAPIEF)," in *Proc. 9th Int. Conf. Inf. Fusion*, Jul. 2006, pp. 1–7.
[21] F. Cuzzolin, "On the properties of the intersection probability," *Ann. Math. Artif. Intell.*, 2007.
[22] J. Dezert and F. Smarandache, "A new probabilistic transformation of belief mass assignment," in *Proc. 11th Int. Conf. Inf. Fusion*, 2008, pp. 1–8.
[23] K. Zhao, Z. Chen, L. Li, J. Li, R. Sun, and G. Yuan, "DPT: An importance-based decision probability transformation method for uncertain belief in evidence theory," *Expert Syst. Appl.*, vol. 213, Mar. 2023, Art. no. 119197.
[24] L. Jiao, F. Wang, Z.-G. Liu, and Q. Pan, "TECM: Transfer learning-based evidential c-means clustering," *Knowl.-Based Syst.*, vol. 257, Dec. 2022, Art. no. 109937.
[25] N. Sghaier, J. Essemine, R. B. Ayed, M. Gorai, R. Ben Marzoug, A. Rebai, and M. Qu, "An evidence theory and fuzzy logic combined approach for the prediction of potential ARF-regulated genes in quinoa," *Plants*, vol. 12, no. 1, p. 71, Dec. 2022.
[26] L. Huang, S. Ruan, and T. Denoux, "Belief function-based semi-supervised learning for brain tumor segmentation," in *Proc. IEEE 18th Int. Symp. Biomed. Imag. (ISBI)*, Apr. 2021, pp. 160–164.
[27] Y. Chen, A. B. Cremers, and Z. Cao, "Interactive color image segmentation via iterative evidential labeling," *Inf. Fusion*, vol. 20, pp. 292–304, Nov. 2014.
[28] S. B. Chaabane, F. Fnaiech, M. Sayadi, and E. Brassart, "Relevance of the Dempster–Shafer evidence theory for image segmentation," in *Proc. 3rd Int. Conf. Signals, Circuits Syst. (SCS)*, Nov. 2009, pp. 1–4.
[29] K. Bisht and A. Kumar, "A portfolio construction model based on sector analysis using Dempster–Shafer evidence theory and Granger causal network: An application to national stock exchange of India," *Expert Syst. Appl.*, vol. 215, Apr. 2023, Art. no. 119434.
[30] H. Cui, L. Zhou, Y. Li, and B. Kang, "Belief entropy-of-entropy and its application in the cardiac interbeat interval time series analysis," *Chaos, Solitons Fractals*, vol. 155, Feb. 2022, Art. no. 111736.
[31] P. Smets and R. Kennes, "The transferable belief model," in *Classic Works of the Dempster-Shafer Theory of Belief Functions*. Berlin, Germany: Springer, 2008, pp. 693–736.
[32] Y. Xue and Y. Deng, "A decomposable Deng entropy," *Chaos, Solitons Fractals*, vol. 156, Mar. 2022, Art. no. 111835.
[33] Y. Yang, X. Pan, and Q. Cui, "An evidence combination rule based on transferable belief model and application in reliability assessment with multi-source data," *IEEE Access*, vol. 8, pp. 69096–69104, 2020.
[34] P. Smets, "The transferable belief model for quantified belief representation," in *Quantified Representation of Uncertainty and Imprecision* (Handbook of Defeasible Reasoning and Uncertainty Management Systems), vol. 1, P. Smets, Eds. Dordrecht, The Netherlands: Springer, 1998.
[35] F. Delmotte and P. Smets, "Target identification based on the transferable belief model interpretation of Dempster–Shafer model," *IEEE Trans. Syst., Man, Cybern. A, Syst. Humans*, vol. 34, no. 4, pp. 457–471, Jul. 2004.
[36] P. Smets, "Application of the transferable belief model to diagnostic problems," *Int. J. Intell. Syst.*, vol. 13, no. 23, pp. 127–157, Feb. 1998.
[37] F. Xiao, "Complex pignistic transformation-based evidential distance for multisource information fusion of medical diagnosis in the IoT," *Sensors*, vol. 21, no. 3, p. 840, Jan. 2021.
[38] P. Smets, "Decision making in the TBM: The necessity of the pignistic transformation," *Int. J. Approx. Reasoning*, vol. 38, no. 2, pp. 133–147, 2005.
[39] F. Voorbraak, "A computationally efficient approximation of Dempster–Shafer theory," *Int. J. Man-Mach. Stud.*, vol. 30, no. 5, pp. 525–536, May 1989.
[40] B. R. Cobb and P. P. Shenoy, "On the plausibility transformation method for translating belief function models to probability models," *Int. J. Approx. Reason.*, vol. 41, no. 3, pp. 314–340, 2006.
[41] R. Jiroušek and P. P. Shenoy, "A new definition of entropy of belief functions in the Dempster–Shafer theory," *Int. J. Approx. Reasoning*, vol. 92, pp. 49–65, Jan. 2018.
[42] R. Jiroušek, V. Kratochvíl, and P. P. Shenoy, "Entropy for evaluation of Dempster–Shafer belief function models," *Int. J. Approx. Reasoning*, vol. 151, pp. 164–181, Dec. 2022.
[43] N. Altwaijry, K. Feki, and N. Minculete, "On some generalizations of Cauchy–Schwarz inequalities and their applications," *Symmetry*, vol. 15, no. 2, p. 304, Jan. 2023.
[44] A. Shternshis, P. Mazzarisi, and S. Marmi, "Measuring market efficiency: The Shannon entropy of high-frequency financial time series," *Chaos, Solitons Fractals*, vol. 162, Sep. 2022, Art. no. 112403.
[45] S. Moral-García and J. Abellán, "Critique of modified Deng entropies under the evidence theory," *Chaos, Solitons Fractals*, vol. 140, Nov. 2020, Art. no. 110112.
[46] D. Dubois and H. Prade, "Properties of measures of information in evidence and possibility theories," *Fuzzy Sets Syst.*, vol. 24, no. 2, pp. 161–182, Nov. 1987.
[47] A. Dempster, "Upper and lower probabilities induced by a multi-valued mapping," *Ann. Math. Statist.*, vol. 38, no. 2, pp. 325–339, 1967.
[48] C. K. Murphy, "Combining belief functions when evidence conflicts," *Decis. Support Syst.*, vol. 29, no. 1, pp. 1–9, 2000.
[49] Y. Deng, W. Shi, Z. Zhu, and Q. Liu, "Combining belief functions based on distance of evidence," *Decis. Support Syst.*, vol. 38, pp. 489–493, Dec. 2004.
[50] K. Yuan, F. Xiao, L. Fei, B. Kang, and Y. Deng, "Modeling sensor reliability in fault diagnosis based on evidence theory," *Sensors*, vol. 16, no. 1, p. 113, Jan. 2016.
[51] Z. Zhang, D. Han, J. Dezert, and Y. Yang, "A new adaptive switching median filter for impulse noise reduction with pre-detection based on evidential reasoning," *Signal Process.*, vol. 147, pp. 173–189, Jun. 2018.
[52] W. Weng and X. Zhu, "INet: Convolutional networks for biomedical image segmentation," *IEEE Access*, vol. 9, pp. 16591–16603, 2021.
[53] C. Rother, V. Kolmogorov, and A. Blake, "'GrabCut' interactive foreground extraction using iterated graph cut," *ACM Trans. Graph*, vol. 23, no. 3, pp. 309–314, 2014.
[54] E. B. Alexandre, A. S. Chowdhury, A. X. Falcao, and P. A. V. Miranda, "IFT-SLIC: A general framework for superpixel generation based on simple linear iterative clustering and image foresting transform," in *Proc. 28th SIBGRAPI Conf. Graph., Patterns Images*, Aug. 2015, pp. 337–344.

[55] X. P. Dong, J. B. Shen, L. Shao, and L. van Gool, "Sub-Markov random walk for image segmentation," *IEEE Trans. Image Process.*, vol. 25, no. 2, pp. 516–527, Feb. 2016.
[56] G. Aletti, A. Benfenati, and G. Naldi, "A semiautomatic multi-label color image segmentation coupling Dirichlet problem and colour distances," *J. Imag.*, vol. 7, no. 10, p. 208, Oct. 2021.
[57] W. Casaca, L. G. Nonato, and G. Taubin, "Laplacian coordinates for seeded image segmentation," in *Proc. IEEE Conf. Comput. Vis. Pattern Recognit.*, Jun. 2014, pp. 384–391.
[58] F. Breve, "Interactive image segmentation using label propagation through complex networks," *Expert Syst. Appl.*, vol. 123, pp. 18–33, Jun. 2019.
[59] S. Zhang, J. H. Liew, Y. Wei, S. Wei, and Y. Zhao, "Interactive object segmentation with inside-outside guidance," in *Proc. IEEE/CVF Conf. Comput. Vis. Pattern Recognit. (CVPR)*, Jun. 2020, pp. 12234–12244.
[60] Q. Huang, J. Sun, H. Ding, X. Wang, and G. Wang, "Robust liver vessel extraction using 3D U-Net with variant dice loss function," *Comput. Biol. Med.*, vol. 101, pp. 153–162, Oct. 2018.
[61] Y. Que, Y. Dai, X. Ji, A. K. Leung, Z. Chen, Z. Jiang, and Y. Tang, "Automatic classification of asphalt pavement cracks using a novel integrated generative adversarial networks and improved VGG model," *Eng. Struct.*, vol. 277, Feb. 2023, Art. no. 115406.
[62] L. Grady, "Random walks for image segmentation," *IEEE Trans. Pattern Anal. Mach. Intell.*, vol. 28, no. 11, pp. 1768–1783, Nov. 2006.

JIAXU ZHANG received the B.S. degree from the College of Science, Northeast Forestry University (NEFU), Harbin, China. He is currently pursuing the master's degree with the School of Electronics and Communication Engineering, Sun Yat-sen University (SYSU), Shenzhen, China. He is currently working with the College Students Innovations Special Project, NEFU. He is recently researching under the research project of "Multimodal Sensors Based xxx" in SYSU. His current research interests include evidence theory, image processing, and machine learning.

XIAOJIAN MA received the B.S. degree in mathematics and applied mathematics from Northeast Forestry University, Harbin, China, in 2000, and the M.S. degree in applied mathematics from the Harbin University of Science and Technology, Harbin, in 2003. She was engaged as an Associate Professor with Northeast Forestry University. Her research interests include uncertainty theory, image processing, and applied statistics.

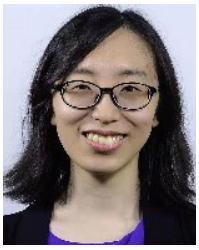

TINGTING SONG (Member, IEEE) received the B.Eng. and M.Phil. degrees from Northeastern University, China, in 2010 and 2012, respectively, and the Ph.D. degree from the School of Engineering, The University of Melbourne, Australia, in 2021. Her main research interests include optical wireless communication system design and digital signal processing.

AO WANG is currently pursuing the B.S. degree with the College of Science, Northeast Forestry University (NEFU). His current research interests include image processing, machine learning, and pattern recognition.

YUHUA LIN is currently pursuing the B.S. degree with the School of Science, Northeast Forestry University (NEFU), Harbin, China. His current research interests include image segmentation and evidential decision support.